Hygroscopicity of Organic Aerosols and Their Contributions to CCN Concentrations Over a Midlatitude Forest in Japan

Deng, Yange

2018-09-16

Deng , Y , Kagami , S , Ogawa , S , Kawana , K , Nakayama , T , Kubodera , R , Adachi , K , Hussein , T , Miyazaki , Y & Mochida , M 2018 , ' Hygroscopicity of Organic Aerosols and Their Contributions to CCN Concentrations Over a Midlatitude Forest in Japan ' , Journal of Geophysical Research : Atmospheres , vol. 123 , no. 17 , pp. 9703-9723 . https://doi.org/10.1029/2017JD027292

http://hdl.handle.net/10138/300144
https://doi.org/10.1029/2017JD027292

unspecified
publishedVersion

Journal of Geophysical Research: Atmospheres

RESEARCH ARTICLE
10.1029/2017JD027292

Hygroscopicity of Organic Aerosols and Their Contributions to CCN Concentrations Over a Midlatitude Forest in Japan

Yange Deng[1], Sara Kagami[1], Shuhei Ogawa[1], Kaori Kawana[2,3], Tomoki Nakayama[4,5], Ryo Kubodera[6], Kouji Adachi[7], Tareq Hussein[8,9], Yuzo Miyazaki[2], and Michihiro Mochida[1,10]

[1]Graduate School of Environmental Studies, Nagoya University, Nagoya, Japan, [2]Institute of Low Temperature Science, Hokkaido University, Sapporo, Japan, [3]Now at Graduate School of Science and Graduate School of Arts and Sciences, University of Tokyo, Tokyo, Japan, [4]Institute for Space-Earth Environmental Research, Nagoya University, Nagoya, Japan, [5]Now at Graduate School of Fisheries and Environmental Sciences, Nagasaki University, Nagasaki, Japan, [6]Graduate School of Science, Nagoya University, Nagoya, Japan, [7]Atmospheric Environment and Applied Meteorology Research Department, Meteorological Research Institute, Tsukuba, Japan, [8]Department of Physics, University of Jordan, Amman, Jordan, [9]Department of Physics, University of Helsinki, Helsinki, Finland, [10]Now at Institute for Space-Earth Environmental Research, Nagoya University, Nagoya, Japan

Key Points:
- Organics contributed to, on average, 38% of the aerosol water uptake
- The hygroscopicity parameter of locally formed fresh BSOA was estimated to be 0.09
- Per 1-μg/m^3 increase of BSOA, the CCN concentration increased 23–299 cm^{-3} at 0.1–0.8% SS

Supporting Information:
- Supporting Information S1

Correspondence to:
M. Mochida,
mochida.michihiro@g.mbox.nagoya-u.ac.jp

Citation:
Deng, Y., Kagami, S., Ogawa, S., Kawana, K., Nakayama, T., Kubodera, R., et al. (2018). Hygroscopicity of organic aerosols and their contributions to CCN concentrations over a midlatitude forest in Japan. *Journal of Geophysical Research: Atmospheres*, *123*, 9703–9723. https://doi.org/10.1029/2017JD027292

Received 13 JUN 2017
Accepted 17 APR 2018
Accepted article online 26 APR 2018
Published online 14 SEP 2018

Abstract The formation of biogenic secondary organic aerosols (BSOAs) in forest environments is potentially important to cloud formation via changes of the cloud condensation nuclei (CCN) activity of aerosols. In this study, the CCN activation of submicrometer aerosols and their chemical compositions and size distributions were measured at a midlatitude forest site in Japan during the summer of 2014 to assess the hygroscopicity of the organic aerosols and their contributions to the local CCN concentrations. The mean number concentrations of the condensation nuclei and CCN at supersaturation (SS) conditions of 0.11–0.80% were 1,238 and 166–740 cm^{-3}, respectively. Organic aerosols and sulfate dominated the submicrometer aerosol mass concentrations. The particle hygroscopicity increased with increases in particle diameters. The hygroscopicity parameter for the organics, κ_{org}, was positively correlated with the atomic O to C ratio. The product of κ_{org} and the volume fraction of OA was 0.12, accounting for 38% of the water uptake by aerosol particles. The hygroscopicity parameter of the locally formed fresh BSOA was estimated to be 0.09. The contribution of OA to the CCN number concentration, which was assessed by subtracting the CCN concentration of the hypothetical inorganic aerosols from that of the ambient aerosols, was 50–182 cm^{-3} for the SS range of 0.11–0.80%. The increase of the CCN number concentrations per 1-μg/m^3 increase of the BSOA was 23–299 cm^{-3} at 0.11–0.80% SS. The contribution of the BSOA to the CCN number concentration can be enhanced by new particle formation.

Plain Language Summary Some of the particles suspended in the atmosphere can absorb water vapors around them and act as nuclei to form cloud droplets. These particles are called *cloud condensation nuclei* (CCN), the quantification of which is important for climate forcing prediction. The ability of a particle to absorb water is referred to as *hygroscopicity*, which is governed by the chemical composition. Volatile organic vapors emitted by vegetation (i.e., biogenic volatile organic compound) after chemical reactions in the atmosphere can either condense onto existing particles or participate in the formation of new particles and thus change the aerosol chemical composition. The aerosol component originated from biogenic volatile organic compounds, named *biogenic secondary organic aerosol* (BSOA), is an important constituent of CCN on a global scale. However, the hygroscopicity of BSOA and its contribution to CCN are not understood well. We performed measurements of the hygroscopicity and chemical composition of aerosol particles in a forest in Japan. Based on the observation, we calculated the hygroscopicity of the BSOA formed in the forest and quantified the contribution of the BSOA to the CCN number concentrations. An enhancement of the contribution of BSOA to the CCN number concentrations by new particle formation is suggested, which is an important subject of future studies.

1. Introduction

Atmospheric aerosols generated from the oxidation of biogenic volatile organic compounds (BVOCs), referred to as *biogenic secondary organic aerosols* (BSOAs), are estimated to account for more than half of the global organic aerosol (OA) flux (TgC/year; Hallquist et al., 2009). The presence of BSOA is estimated to

increase the global annual mean concentration of cloud condensation nuclei (CCN) by 3.6–45.2% under a water vapor supersaturation (SS) condition of 0.2% (Scott et al., 2014). Hence, BSOA could affect cloud properties and thus the estimation and interpretation of the Earth's changing energy budget (Scott et al., 2014). Moreover, the role of BSOA in CCN formation is important for understanding the biosphere-aerosol-climate interaction (Carslaw et al., 2010; Paasonen et al., 2013). While laboratory studies of CCN activity with modeled BSOA (e.g., Alfarra et al., 2013; Engelhart et al., 2008; Frosch et al., 2011, 2013; Lambe et al., 2011; Lang-Yona et al., 2010; Massoli et al., 2010) are essential to revealing the activation properties of particles generated from specific precursors, field studies are important for understanding CCN properties under complex atmospheric conditions. BSOA could exist in abundance in forest aerosols as a result of the large emission of BVOC from dense vegetation. Intensive field studies of CCN properties have been performed in a boreal forest in Finland (Cerully et al., 2011; Paramonov et al., 2013; Sihto et al., 2011) and in an Amazonian tropical forest (Gunthe et al., 2009; Roberts et al., 2001, 2002). There are also several studies that were carried out in North America (Levin et al., 2012, 2014; Pierce et al., 2012; Shantz et al., 2010), the southeastern United States (Cerully et al., 2015), Europe (Dusek et al., 2010; Wu et al., 2013), a Southeast Asian rainforest (Irwin et al., 2011), and East Asia (Kawana et al., 2017).

The hygroscopicity of aerosol particles, which relates to their chemical compositions, and the size of the particles are the two key parameters that determine CCN activity (Farmer et al., 2015; Petters & Kreidenweis, 2007). The hygroscopicity of aerosol particles and respective chemical components are commonly represented by the parameter κ. Whereas the estimated global average κ of aerosol particles over continental areas is 0.3 (Gunthe et al., 2009, and references therein), the aerosols over forest environments are in general less hygroscopic (Cerully et al., 2011, 2015; Gunthe et al., 2009; Irwin et al., 2011; Levin et al., 2014; Paramonov et al., 2013). Furthermore, the smaller particles in forest environments are generally less hygroscopic than the larger particles, although some instances of the opposite characteristics have also been observed (Irwin et al., 2011). The contribution of organics to the observed aerosol hygroscopicity can be substantial in forest environments as a result of the dominance of OAs (Cerully et al., 2011; Gunthe et al., 2009; Levin et al., 2014; Pierce et al., 2012). Unlike inorganics, which have well-understood hygroscopicity, our understanding of the hygroscopicity of organics is far from complete due to the complexity in their composition. For this reason, the hygroscopicity of organics should be studied further over different forest environments with different precursor emissions from different vegetation. The variations of the hygroscopicity parameters of organics (κ_{org}) has been represented using the atomic O to C ratio (O:C), which serves as an indicator of the oxidation level of the organics, both in laboratory studies (Frosch et al., 2011; Jimenez et al., 2009; Lambe et al., 2011; Massoli et al., 2010) and forest field studies (Cerully et al., 2015; Wu et al., 2013). However, further investigations are needed to be able to draw a conclusion about the relationship of κ_{org} and the O:C ratio.

There are two mechanisms by which BSOA contributes to the number concentration of CCN. One is the promotion of the formation of new particles by participating in nucleation and by suppressing coagulation of the newly formed particles as a result of the growth by condensation or formation in the particles. The other is the enhancement of the CCN activity of newly formed and preexisting aerosol particles due to the increase in the solute mass by the addition of BSOA via condensation or formation in the particles. Both laboratory (Kirkby et al., 2016; Riccobono et al., 2014; Tröstl et al., 2016; Zhao et al., 2013) and field (Bianchi et al., 2016) studies have revealed the role of oxidized organic vapors in the nucleation and initial particle growth. Other studies have reported the contributions of the condensation of low volatility biogenic organic vapors to the growth of newly formed particles in the CCN size range (e.g., Yu et al., 2014; Zhou et al., 2015). In Amazon, where new particle formation (NPF) events were only observed in the wet season in an open pasture site (Wimmer et al., 2017), the enhancement of the solute mass is expected to be the main mechanism through which BSOA contribute to CCN number concentrations. In other forests, where NPF events were frequently observed, including in a boreal forest in Finland (Sihto et al., 2011), a forested mountainous area in Colorado (Levin et al., 2012), an Ozark forest in the Central United States (Yu et al., 2014), and during the intensive BSOA nucleation/condensation episode in Whistler Mountain Valley in western Canada (Pierce et al., 2012), BSOA may contribute to the increase of the CCN number concentration by promoting the NPF as well. Given that previous model calculations have indicated that nearly half of the low-level cloud CCN are derived from NPF on a global scale (Merikanto et al., 2009), the contribution of BSOA to CCN concentrations should be better understood in relation to the occurrence or absence of NPF events.

This study aims to illustrate the hygroscopicity of OA and BSOA and the influence of OA and BSOA on CCN concentrations in a midlatitude forest in Japan. Previous studies based on a 10-day observation of the forest have indicated that NPFs occurred frequently under maritime air mass conditions and potentially contributed to the increase of CCN concentrations during the daytime and that the growth of these newly formed particles was primarily caused by organics originating from locally formed BSOA (Han et al., 2013, 2014; Kawana et al., 2017). Furthermore, the hygroscopicity parameter κ of the newly formed Aitken mode particles was calculated (Kawana et al., 2017). Based on a longer (32 days) field study in the summer of 2014, this study expands on the previous studies to further illustrate the hygroscopicity of the forest OA, including its diurnal variation and relation to the O:C ratio, and to assess the contributions of OA/BSOA to the overall aerosol hygroscopicity and CCN number concentrations. This study also assesses the influence of NPF on the contributions of OA/BSOA to the CCN number concentrations.

2. Atmospheric Observations

Atmospheric observations were performed at the Wakayama Forest Research Station of Kyoto University (34.06°N, 135.52°E, approximately 500 m above sea level), which is located in the central part of the Kii peninsula, facing the western North Pacific, in 2014. The study period of this work was from 28 July to 28 August, during which CCN data were obtained. The nearest megacity, Osaka (with 2.7 million inhabitants), is approximately 70 km to the north of the study site, and the North Pacific is approximately 60 km to the southeast. Coniferous trees of *Cryptomeria japonica*, *Chamaecyparis obtusa*, and *Pinus densiflora* are broadly distributed in the Kii peninsula. Broad-leaf trees, such as *Quercus serrata* and *Quercus crispula*, are also distributed (Okumura, 2009). The concentrations of VOCs and inorganic gaseous species in the studied forest in a part of the studied period are reported elsewhere (Ramasamy et al., 2016).

During the observation period, a size-resolved CCN measurement system, a scanning mobility particle sizer (SMPS), and a high-resolution time-of-flight aerosol mass spectrometer (AMS, Aerodyne Research, Inc.) shared the same inlet tubing (1/2-inch outside diameter, stainless steel tubing), the upper end of which was approximately 7.5 m above the ground. A $PM_{2.5}$ cyclone (URG) was installed at the lower end of the inlet tubing. An assisting pump (ULVAC, DA30S) was used to keep the total sample flow rate at 16.7 L/min. The aerosol flow upstream of the CCN system was dried with two diffusion dryers, in series, one using silica gel and the other using molecular sieves. The aerosol flow to the SMPS and AMS was dried with two diffusion dryers containing silica gel. During the observation period subjected to the analysis, the relative humidity (RH) at the outlets of the excess flows of the differential mobility analyzers (DMAs) in the CCN system and in the SMPS, and the RH of the assistant flow of the AMS were $<$12%, $<$12%, and $<$2%, respectively.

In the CCN measurement system, polydisperse aerosols were passed through a DMA (DMA, 3080, 3081, TSI, with a sheath flow rate of 8.0 L/min and a sheath to sample flow ratio of 10) to obtain monodisperse aerosols. The monodisperse aerosol flow was then divided into two branched flows. One, with a flow rate of 0.5 L/min, was directed to the CCN counter (CCN-100, DMT, with a sheath to sample flow ratio of 10) to measure the CCN number concentrations with four different SS settings. The other, with a flow rate of 0.3 L/min, was directed to a condensation particle counter (CPC, 3025A, TSI) to measure the concentrations of the monodisperse aerosol particles. Under each SS condition, 17 different diameters (size range: 20.2–299.6 nm) were selected to obtain a CCN efficiency spectrum. The diameter setting of the DMA was fixed at each diameter for 3 min; the data in the first 30 s were not used. The waiting time after the change of the SS conditions was in the range of 8–10 min. Consequently, it took 1 hr to obtain the CCN activation spectrum at each of the four SSs and 4 hr to obtain the full set of CCN spectra. Before the atmospheric observations, an aqueous solution of pure ammonium sulfate (AS; 99.999% purity, Sigma-Aldrich) was nebulized, and the generated aerosol was introduced to the CCN system and subjected to the same analysis procedures as the ambient aerosols. The activation diameters (d_{act}) of the AS under different SS settings were obtained (section 3.1) and were then used to determine the actual SS conditions by inputting the d_{act}, the average temperature at the top of the CCN column during the ambient observation and on-site calibration (299 K), and AS volume fraction of unity in the Köhler calculation page of the online Extended AIM Aerosol Thermodynamics Model II (E-AIM II, http://www.aim.env.uea.ac.uk/aim/model2/model2a.php; Clegg et al., 1998; Wexler & Clegg, 2002). Note that the molar volumes of the dry inorganic salts, and the equations to calculate the density and surface tension of pure water for off-line analysis are same as the ones used in the online E-AIM II model. The calibrated SSs were 0.11%, 0.24%, 0.42%, and 0.80%.

The SMPS, which is composed of a DMA (DMA, 3080, 3081, TSI) and a CPC (3775, TSI), was used to obtain the aerosol number-size distributions. The sample flow rate was 0.3 L/min, and the sheath to sample flow ratio was 10. The dry mobility diameter range was 13.8–749.9 nm, and the time resolution was 5 min. The AMS was operated in alternating V (MS and PToF modes) and W modes (MS mode) to obtain the bulk and size-resolved chemical compositions of nonrefractory aerosol components (organics, sulfate, ammonium, nitrate, and chloride) at a time resolution of half an hour. The O:C and H:C (atomic ratio of H to C) ratios were derived based on high-resolution analyses of the W-mode data. A detailed description of the AMS is presented by DeCarlo et al. (2006). Composition-dependent collection efficiency (Middlebrook et al., 2012) was applied for quantification. The AMS- and SMPS-derived volume concentrations of the aerosols correlated strongly (r: 0.98; slope of the regression line: 1.14; supporting information Figure S1). The accuracy of the sizing using the DMAs was assessed using size standard particles with the procedure in Kawana et al. (2014). The AMS was calibrated on-site. The performance of the DMAs and the details in the AMS calibrations are presented in Text S1.

A second tubing (1/2-inch outside diameter), whose inlet was also approximately 7.5 m above the ground, was used to introduce the ambient air to a single wavelength particle soot absorption photometer (1λ-PSAP, 567 nm, Radiance Research Inc.) after the air passed through a PM_1 cyclone (URG), a diffusion dryer containing silica gel, and a stainless steel tube heated to 300 °C (Guo et al., 2014). The mass concentrations of submicrometer black carbon (BC) were calculated from the absorption coefficient of the aerosol measured by the PSAP, according to the method of Kondo et al. (2009).

Further, aerosol samples were collected using a two-stage impactor sampler (AS-16W, Arios) (Adachi et al., 2016) and a high-volume sampler (Model 120SL, Kimoto Electric) equipped with a cascade impactor (Model TE-234, Tisch Environmental). Aerosol samples collected using the two-stage impactor sampler were used for transmission electron microscopy analysis. The samples collected on backup filters placed in the high-volume sampler (50% cutoff diameter, 0.95 μm) were used for the quantification of water-soluble organic carbon and inorganic ions (ammonium, nitrate, nitrite, sulfate, sodium, potassium, calcium, magnesium, and chloride) using a total organic carbon analyzer (Model TOC-L_{CHP}, Shimadzu) and an ion chromatograph (Model 761 compact IC, Metrohm) (Müller et al., 2017), respectively. Details about the collection and analysis of the samples are presented in Text S2. Meteorological data were collected at Wakayama Forest Research Station. Data of temperature and RH of ambient air (HMP-155, Vaisala), precipitation (RH-5E, IKEDA-KEIKI), and solar radiation (CMP3-L, Campbell) were used in this study (Kyoto University, 2015, 2016).

3. Data Analysis

3.1. CCN Activation Curve

The obtained CCN activation spectra, that is, the raw size-resolved CCN to condensation nuclei (CN; all the particles measured using CPC 3025A) concentration ratio ($f_{N_{CCN}/N_{CN},meas}$), were first corrected for the presence of multiply (doubly and triply) charged particles with methods similar to those of Mochida et al. (2010). For the estimation of the multiply charged particles, 1-hr averages of the number-size distributions of the ambient particles, derived from the SMPS's software (Aerosol Instrument Manager; TSI, Inc.), were used.

The corrected CCN activation spectra ($f_{N_{CCN}/N_{CN},corr}$) were fit with a cumulative Gaussian distribution function (Rose et al., 2008) with weighting by the standard deviation (SD) of the measured CCN to CN concentration ratios at each $f_{N_{CCN}/N_{CN},meas}$ data point and with consideration for the shape of the DMA transfer functions. The fitting function f_{fit} is as follows:

$$f_{fit} = a\left[1 + \mathrm{erf}\left(\frac{d_{dry} - d_{act}}{\sigma_a\sqrt{2}}\right)\right] \quad (1)$$

where erf is the error function; a is half of the upper asymptote of f_{fit}; d_{dry} is the dry particle diameter; d_{act} is the activation diameter, which is the particle diameter at f_{fit} = a/2; and σ_a is the SD of the cumulative Gaussian distribution function. The weighting factor f_w is

$$f_w = \left(f_{N_{CCN}/N_{CN},meas}\sqrt{\frac{1}{n_{CCN}} + \frac{1}{n_{CN}}}\right)^{-1} \quad (2)$$

where n_{CCN} and n_{CN} represent the CCN and CN counts, respectively.

The fitting is to find the most appropriate combination of a, d_{act}, and σ_a in equation (1) when the Q in equation (3) reaches its minimum.

$$Q = \sum_i \left\{ \left[f_{N_{CCN}/N_{CN},corr} - \int f_{fit}(d_{dry}) \left(\frac{dN_{1+}}{d\log d_{dry}} \right) \Omega_i(\log d_{dry}) d\log d_{dry} / \int \left(\frac{dN_{1+}}{d\log d_{dry}} \right) \Omega_i(\log d_{dry}) d\log d_{dry} \right] f_w \right\}^2 \quad (3)$$

where $f_{fit}(d_{dry})$ is f_{fit}, represented as a function of d_{dry}; $dN_{1+}/d\log d_{dry}$ is the calculated number-size distribution of the +1 charged particles entering the CCNC and CPC 3025A in a hypothetical case that all +1 charged particles pass through the DMA, regardless of size; and $\Omega_i(\log d_{dry})$ is the transfer function of the DMA of the ith size bin (Stolzenburg, 1988). The $\int f_{fit}(d_{dry}) \left(\frac{dN_{1+}}{d\log d_{dry}} \right) \Omega_i(\log d_{dry}) d\log d_{dry}$ and $\int \left(\frac{dN_{1+}}{d\log d_{dry}} \right) \Omega_i(\log d_{dry}) d\log d_{dry}$ are, respectively, the calculated CCN and CN number concentrations in the sample flow entering the CCNC and CPC3025A, which were derived using the transfer function of the DMA.

If the $|f_{fit} - f_{N_{CCN}/N_{CN},corr}|$ at a given size is greater than 0.3, the corresponding f_w is forced to be 0 and the fitting is repeated. In total, 166, 170, 176, and 175 effective spectra were obtained (Text S3) during the observations under 0.11%, 0.24%, 0.42%, and 0.80% SS, respectively.

3.2. Hygroscopicity of Aerosol Particles and Organic Components

The κ- Köhler theory (Petters & Kreidenweis, 2007) was adopted to calculate the hygroscopicity of the measured ambient aerosol particles. In the theory, the water vapor saturation ratio over the aqueous droplets, S, is represented by

$$S = \frac{d_{wet}^3 - d_{act}^3}{d_{wet}^3 - d_{act}^3(1 - \kappa_t)} \exp\left(\frac{4\sigma M_w}{RT\rho_w d_{wet}} \right) \quad (4)$$

where d_{wet} is the wet particle diameter, d_{act} is the dry particle activation diameter (section 3.1), κ_t represents the hygroscopicity of the dry aerosol particles, ρ_w is the density of water, M_w is the molecular weight of water, σ is the surface tension at the solution/air interface, R is the universal gas constant, and T is the temperature in Kelvin. In this study, T is represented by the average of the temperature at the upper end of the CCNC column (299 K) and σ is represented by the temperature-dependent surface tension of pure water. The SS value above the droplet surface is represented as $S - 1$. For a known d_{act}, κ_t was obtained by varying κ_t until the maximum SS from equation (4) became closest to the SS of the CCN counter with a resolution of κ_t of 0.001 (Rose et al., 2010).

The hygroscopicity of the OA components (κ_{org}) was calculated assuming the volume additivity of the water taken up by each component (i.e., the Zdanovskii-Stokes-Robinson [ZSR] assumption; Petters & Kreidenweis, 2007), which is written as follows:

$$\kappa_t = \varepsilon_{org}\kappa_{org} + \varepsilon_{inorgsalt}\kappa_{inorgsalt} + \varepsilon_{BC}\kappa_{BC} = \varepsilon_{org}\kappa_{org} + \sum_{i=1}^{4} \varepsilon_i\kappa_i + \varepsilon_{BC}\kappa_{BC} \quad (5)$$

where ε_{org}, $\varepsilon_{inorgsalt}$, and ε_{BC} are the respective volume fractions and κ_{org}, $\kappa_{inorgsalt}$, and κ_{BC} are the respective hygroscopicity parameters of organics, inorganic salts, and BC. The i ranges from 1 to 4, representing the four species of inorganic salts (ammonium nitrate, AS, ammonium hydrogen sulfate, and sulfuric acid). ε_i is the volume fraction of each inorganic salt i. ε_{org}, ε_i, and ε_{BC} were calculated based on the size-resolved mass concentrations of the organics, sulfate, nitrate, and ammonium from the AMS measurements and the submicrometer BC mass concentrations from the PSAP measurements. BC was assumed to be internally mixed with other aerosol components and have the same mass-size distribution as the organics. The density of organics (ρ_{org}) was estimated to be 1.4 ± 0.1 g/cm^3 using the AMS-derived O:C and H:C ratios of organics (Kuwata et al., 2012) and the mean value of 1.4 g/cm^3 was adopted for the study. The density of BC was assumed to be 1.77 g/cm^3 (Park et al., 2004). Note that the results from the filter-based analysis (Table S5) indicate that the contribution of sea salt and minerals to the mass concentration of submicrometer aerosol was small. More details about the calculations of the volume fractions of each chemical component are presented in Text S4. The derivation of the hygroscopicity parameter of each inorganic salt (κ_i)

using the E-AIM II model and the evaluation of the ZSR assumption for the estimation of the hygroscopicity parameter of the mixtures of inorganic salts ($\kappa_{inorgsalt}$) are presented in Text S5. The κ_{BC} was assumed to be 0.

Furthermore, the hygroscopicity parameter of the locally formed fresh BSOA (κ_{BSOA}) was estimated. For this estimation, the observed OAs were assumed to be composed of the locally formed fresh biogenic aerosols (fresh BSOA) and regionally transported OAs (regional OA; Han et al., 2014). The influence of the primary anthropogenic emissions is expected to be small at this remote site (Han et al., 2014); the primary biological aerosol particles such as fungal spores and plant debris, which were reported to be present at the study site (Zhu et al., 2016), are expected to be present mainly in the super-micrometer size range (as is the case in an Amazonian forest during the wet season; Pöschl et al., 2010). To estimate the mass concentrations of fresh BSOA (m_{BSOA}) and regional OA (m_{ROA}), the period of 0600–0900 Japan standard time (JST), when the mass concentration of OA reached its daily minimum, was defined as the background period. The m_{ROA} during 0600–0900 JST was estimated as the mean OA mass concentration during the period ($m_{ROA,6-9}$). During other periods of the day, the m_{ROA} were calculated as the averages of the $m_{ROA,6-9}$ values before and after the time period of interest. The fresh BSOA is defined as the difference between the mass concentration of OA and m_{ROA}. The estimation was based on the assumption that the increase of OA in the daytime was mainly contributed by the secondary formation of biogenic aerosol. Note that the decreasing trend of the mass concentration of OA from midnight to ~0900 JST (Figure 2) suggests that the shoulder of the peak of OA in the previous day, probably originated from locally formed but aged BSOA, could also contribute to the estimated m_{ROA} to some extent. A possible positive bias of m_{BSOA} by the secondary formation of anthropogenic OA was estimated to be in general within a factor of 2.4, as assessed in Text S6. The κ_{BSOA} was then calculated based on the assumption that κ_{org} is the sum of the products of the κ of the OAs and their respective mass fractions.

$$\kappa_{org} = f_{ROA}\kappa_{ROA} + f_{BSOA}\kappa_{BSOA} \tag{6}$$

Here f_{ROA} and f_{BSOA} are, respectively, the mass fractions of regional OA and fresh BSOA in the total OA measured using the AMS. The hygroscopicity parameter of the regional OA (κ_{ROA}) was assumed to be constant throughout the observation period: The κ_{ROA} under each SS condition were the mean κ_{org} under that SS condition during 0500–0900 JST over the whole study period. The resulting κ_{ROA} values at 0.11%, 0.23%, 0.42%, and 0.80% SS were 0.33, 0.23, 0.31, and 0.23, respectively.

3.3. Contributions of Organics to CCN Concentrations

Both organic and inorganic components contribute to the aerosol CCN activity by their water uptake. Consequently, the CCN number concentrations are also contributed by these components. To assess the contributions of OA to the CCN concentrations, we assumed a hypothetical case that the organic components in respective particles in the studied aerosols are omitted. The diameter of the hypothetical inorganic aerosol particles (d_{inorg}) was derived from d_{dry} and the volume fractions of organics (ε_{org}) or inorganics (ε_{inorg}).

$$\frac{\pi {d_{inorg}}^3}{6} = \frac{\pi {d_{dry}}^3}{6}\varepsilon_{inorg} = \frac{\pi {d_{dry}}^3}{6}\left(1 - \varepsilon_{org}\right) \tag{7}$$

$$d_{inorg} = d_{dry}\left(\varepsilon_{inorg}\right)^{1/3} \tag{8}$$

Note that the inorganics here include both inorganic salts and BC. This assumption is based on the fact that most of the studied aerosol particles were internal mixtures of inorganics and organics, as shown by the transmission electron microscopy images (Figure S4) and by the unimodal hygroscopic growth factor distributions observed in an earlier study at the same site in the same season of 2010 (Kawana et al., 2017). The mass-size distributions from the AMS measurement at the 1-hr time resolution was used to calculate the ε_{org} (Text S4 and Table S2) of the aerosol particles in the four d_{act} ranges under the four different SS conditions. The patterns and magnitudes of the number-size distributions of the hypothetical inorganic particles were same as those of the ambient particles but were shifted to a smaller size range. The activation diameter of the pure inorganic particles, $d_{act,inorg}$, was derived by applying κ_{inorg} instead of κ_t to equation (4).

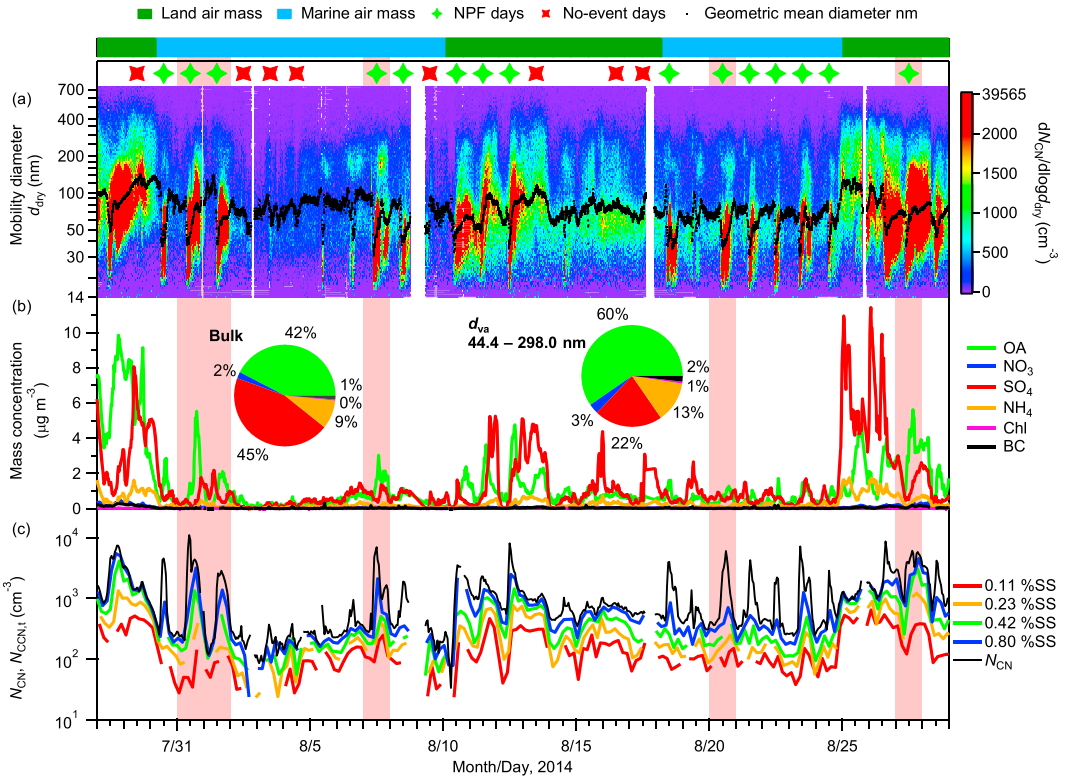

Figure 1. Time series of (a) the aerosol number-size distributions and the geometric mean diameters; (b) the mass concentrations of organics (organic aerosol [OA]), sulfate (SO_4), nitrate (NO_3), ammonium (NH_4), chloride (Chl), and black carbon (BC); and (c) the aerosol number concentrations (N_{CN}) and cloud condensation nuclei (CCN) number concentrations under four different supersaturation (SS) conditions. The pie charts in panel b present the fractions of the average mass concentrations of chemical components of the bulk aerosols and the aerosols in the d_{va} range of 44.4–298.0 nm over the whole study period. At the top of the graph, the dominant air masses and new particle formation (NPF) and no-event days are indicated. The 5 days selected for the calculation of κ_{BSOA} (section 4.3) are shaded in pink.

The CCN number concentrations of the hypothetical inorganic aerosols ($N_{CCN,inorg}$) were obtained by integrating their respective number-size distributions above their respective $d_{act,inorg}$. Furthermore, the number concentration of ambient CCN ($N_{CCN,t}$) was calculated by integrating the ambient aerosol number-size distribution greater than the measured activation diameter (d_{act}), assuming internally mixed aerosol particles. The obtained $N_{CCN,t}$ was 0.95–0.97 times that found by integrating the product of the ambient number-size distribution and the simultaneous corrected activation spectrum ($f_{N_{CCN}/N_{CN},corr}$) across the whole measured SMPS size range (Figure S5); we consider $N_{CCN,t}$ to be accurate enough to evaluate the contribution of organics to the CCN number concentration. $N_{CCN,org}$ was defined as the difference of the CCN number concentrations of the ambient aerosols ($N_{CCN,t}$) and those of the hypothetical inorganic aerosols ($N_{CCN,inorg}$), that is, the enhancement of the CCN number concentration in the presence of OA. The contribution of OA to the total CCN concentrations was evaluated using $N_{CCN,org}$ and the ratio $N_{CCN,org}/N_{CCN,t}$. Note that CCN number concentrations are not linear to the mass concentrations of respective chemical components. Hence, the approach using $N_{CCN,inorg}$, $N_{CCN,org}$, and $N_{CCN,org}/N_{CCN,t}$ is a sensitivity analysis.

The contribution of the locally formed fresh BSOA to the $N_{CCN,org}$, referred to as $\Delta N_{CCN,org}$, was estimated as the difference between the obtained $N_{CCN,org}$ and its background values. Similarly, the contribution of the freshly formed secondary component to $N_{CCN,t}$ ($\Delta N_{CCN,t}$) was estimated as the difference between $N_{CCN,t}$ and its background values. The estimates of the background values of $N_{CCN,org}$ and $N_{CCN,t}$ are detailed in Text S7.

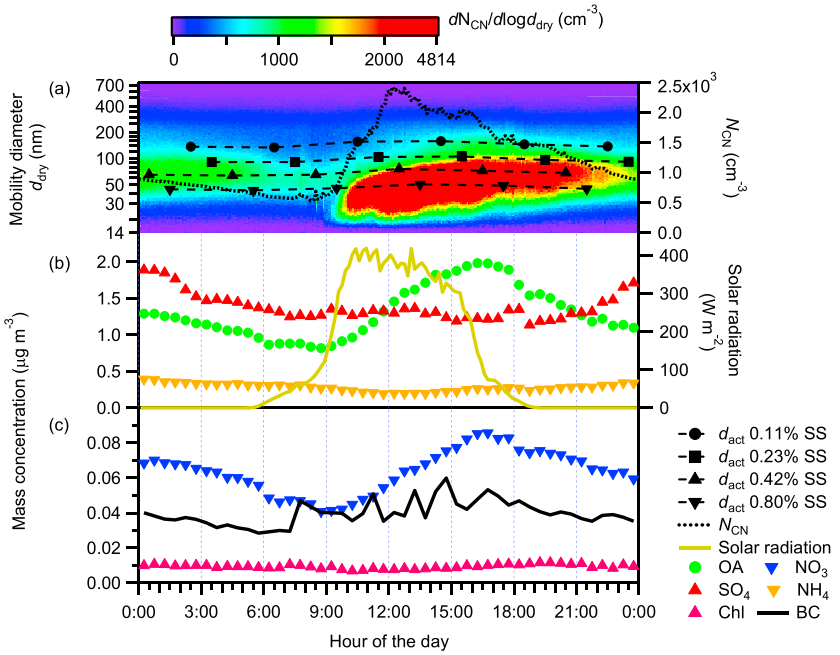

Figure 2. Diurnal variations of (a) the aerosol number-size distributions and (b and c) the mass concentrations of the chemical components. The cloud condensation nuclei activation diameters (d_{act}) under the four different supersaturation (SS) conditions (left axis), and the total aerosol number concentrations (N_{CN}, right axis) are superimposed in panel a. The diurnal variation of solar radiation is superimposed in panel b (right axis). All data are averages over the whole study period. BC = black carbon; OA = organic aerosol.

4. Results and Discussion

4.1. General Characteristics of the Studied Aerosols

The time series of the aerosol number-size distributions and the mass concentrations of the different aerosol chemical components, as well as the CCN number concentrations at the four different SS conditions are presented in Figure 1. The variations of these parameters across the observation period and on a diurnal scale on NPF days (as indicated by green plus symbols at the top of Figure 1; see the discussion below and Text S8 for details) are evident. The mean ± SD of the geometric mean diameters calculated from the aerosol number-size distributions was 74 ± 20 nm (Figure 1a). The hourly means of the aerosol number concentrations (N_{CN}) ranged from 34 to 1.1 × 10^4 cm^{-3} (Figure 1c) and the mean ± SD for the entire period (time resolution: 5 min) was 1,238 ± 1,468 cm^{-3}. Sulfate, organics, and ammonium dominated the submicrometer nonrefractory aerosol components (Figure 1b). The mean ± SD of the mass concentrations of the sulfate, organics, and ammonium were 1.38 ± 1.79, 1.31 ± 1.70, and 0.28 ± 0.33 μg/m^3, respectively. The sum of the nitrate, BC, and nonrefractory chloride accounted for only 3.6% of the observed submicrometer aerosol mass, on average. The contribution of other refractory materials including sea salt to the submicrometer aerosol mass (diameter: <0.95 μm) was negligible (Table S5). In the vacuum aerodynamic diameter range that corresponded to the dry activation diameter range under SS conditions of 0.11–0.80% (d_{va}: 44.4–298.0 nm), OA accounted for a much higher proportion (60%) than sulfate (22%) and other inorganic components. While the CCN number concentrations are influenced by the chemical compositions and size distributions of the aerosols (Wang et al., 2008), their patterns of variations followed the patterns of the measured aerosol number concentrations, especially at high-SS conditions (Figure 1c): the correlation coefficients r between $N_{CCN,t}$ and N_{CN} at 0.11%, 0.24%, 0.42%, and 0.80% SS were 0.33, 0.59, 0.63, and 0.85, respectively. The mean ± SD of the CCN number concentrations at 0.11%, 0.24%, 0.42%, and 0.80% SS were 166 ± 133, 291 ± 265, 487 ± 556, and 740 ± 852 cm^{-3}, respectively. An air mass trajectory analysis using NOAA's HYSPLIT atmospheric transport and dispersion modeling system (Draxler et al., 1997; Draxler & Hess, 1998) shows that the air masses were transported from the North Pacific, terrestrial regions (Asian continent and Japan archipelago), or both (Figure S6). The dominant air mass origins are indicated at the top of Figure 1. When the air masses were

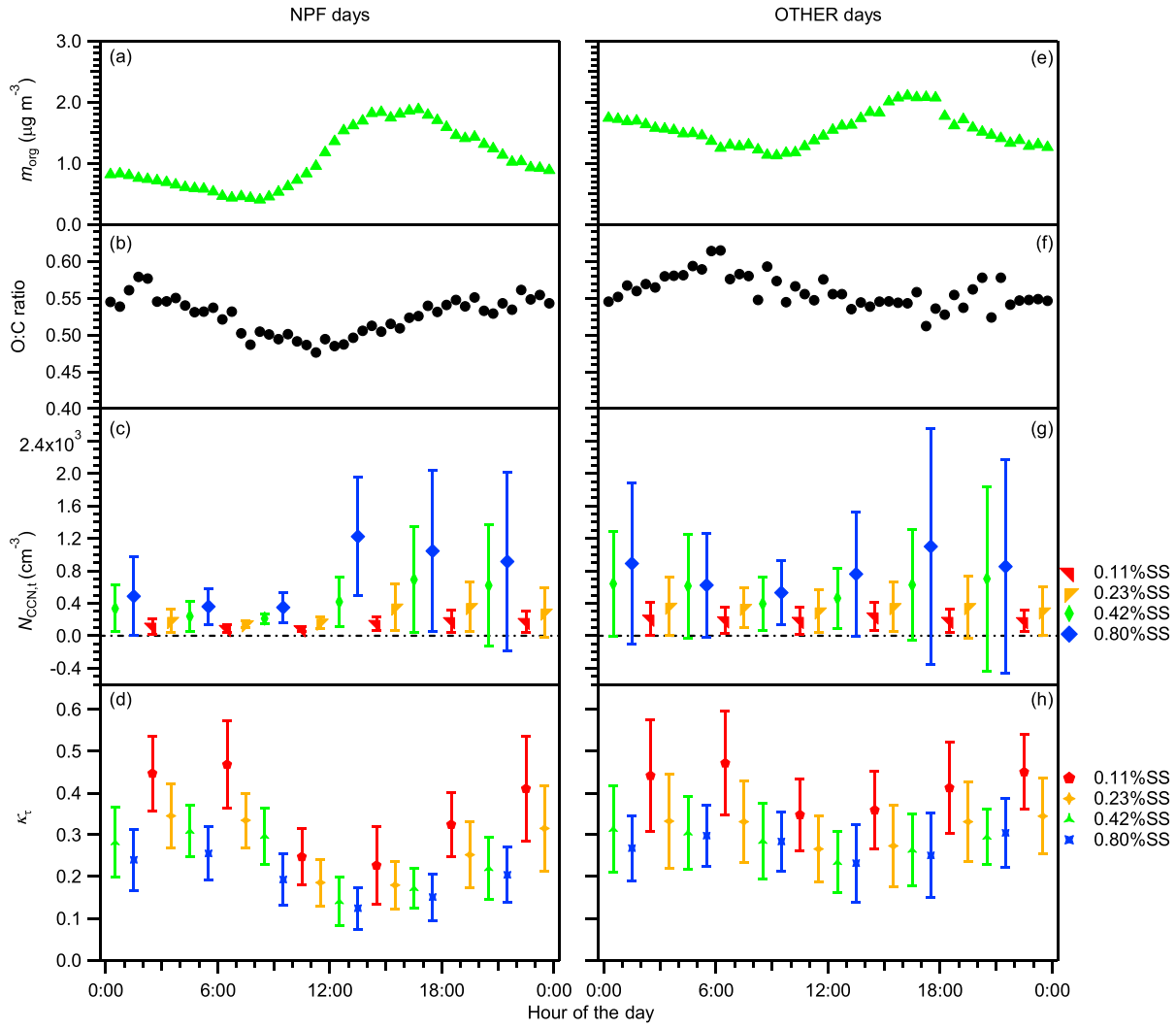

Figure 3. Diurnal variations of (a and e) the organic mass concentrations, (b and f) O:C ratios of organics, (c and g) cloud condensation nuclei (CCN) number concentrations ($N_{CCN,t}$), and (d and h) particle hygroscopicity (κ_t) over the whole study period. Panels a, b, c, and d show NPF days, and panels e, f, g, and h show OTHER days. The whiskers in panels c, g, d, and h represent the standard deviations. NPF = new particle formation; SS = supersaturation.

from the terrestrial regions, the daily averages of the aerosol numbers and mass concentrations tended to be higher than those on days when the air masses were from the Pacific (Figures 1a and 1b). The results suggest that both the aerosol number and mass concentrations were influenced by the inflowing long-range transported air masses.

The diurnal variations of the number-size distributions of the aerosols and the mass concentrations of the chemical components over the whole study period are presented in Figure 2. Both the aerosol number concentrations (Figure 2a) and the mass concentrations of OA (m_{org}, Figure 2b) showed daily minima between 0600 and 0900 JST and increased considerably after the minima. N_{CN} reached its maximum at approximately 1300 JST, and m_{org} reached its maximum 4 hr later, at approximately 1700 JST. Photochemical reactions after sunrise should have led to the formation of BSOA and thus the growth of particles; the latter was suggested by the diurnal variations of the aerosol number-size distributions (Figure 2a). The average dry activation diameters (d_{act}) under all of the four SS conditions increased with the increase of m_{org}, indicating the decrease of the aerosol hygroscopicity by the formation of BSOA. The diurnal variation pattern of sulfate (Figure 2b) was not evident, although a maximum was observed at midnight. Ammonium (Figure 2c) presented a daily minimum at noon. Nitrate (Figure 2c) presented a similar diurnal pattern as that of organics. The mass

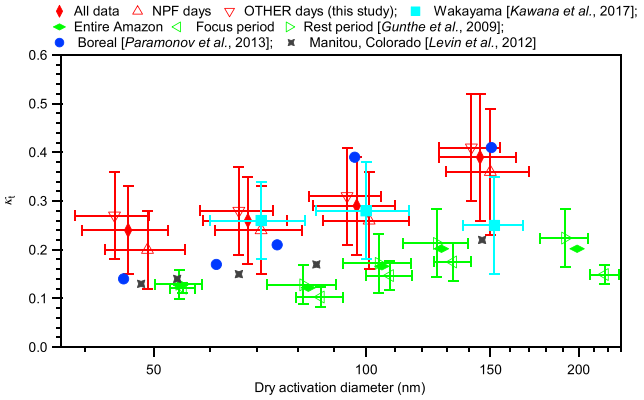

Figure 4. The κ_t of the studied aerosol particles and those from other studies. Red markers represent the results from this study for (open triangles) NPF days, (open squares) OTHER days, and (filled circles) the entire period. Green markers represent the results from the study during the Amazon's rainy season by Gunthe et al. (2009), during the (open triangles) focus period with minimal influences from long-range transport or local pollution, (open squares) the rest period, and (filled circles) the entire study period. Blue markers represent the results from the boreal forest (Paramonov et al., 2013). Black markers represent the results from the semiarid mountainous forest in Western Canada (Levin et al., 2012). Light blue markers represent the results of the 2010 campaign at the same observation site as used in this study (Kawana et al., 2017). The horizontal and vertical whiskers represent the standard deviations of the dry activation diameters and κ_t, respectively. NPF = new particle formation; SS = supersaturation.

concentrations of BC increased in the daytime (Figure 2c), which may have been influenced by the charring of organics at the heating temperature of 300 °C during the measurement.

As was found during the 2010 campaign (Han et al., 2013), frequent NPF events were observed. To assess the contributions of the formation of new particles to CCN, the entire observation period was categorized into NPF days (15 days), no-event days (8 days), and the remaining days (9 days), on which weak NPF may have occurred (Figures 1 and S5). Note that, unlike in the year of 2010, when NPF events only occurred at the arrival of marine air masses, NPF events were also observed when the air masses were from the terrestrial regions (Figures 1 and S6). The SMPS-derived particle number-size distributions and the mode diameter of the mode in the smaller side from the double-mode lognormal fitting to the distributions (Hussein et al., 2005) were used to define NPF and no-event days (details are given in Text S8). Additionally, the no-event days and the remaining days were combined and called *OTHER days* (17 days) for the analysis. Figures 3a and 3e present the diurnal variations of the organic mass concentrations on NPF days and OTHER days, respectively. On NPF days, the mass concentrations of OA in the afternoon hours increased by up to more than four times the daily minimum (0.40 $\mu g/m^3$, 0600–0900 JST). On OTHER days, the relative enhancements of the OA mass concentrations were weaker: The afternoon maximum was less than twice the morning minimum. The absolute increases of the OA masses on NPF days and OTHER days were 1.5 and 1 $\mu g/m^3$, respectively. The different magnitudes of the increases in the OA mass concentrations on NPF days and OTHER days could be explained by the stronger day/night variations of solar radiation, air temperature, and RH on NPF days compared to those on OTHER days (Figures S7 and S8). The contrast of the meteorological conditions is more obvious when NPF and no-event days are compared (Figure S8). On NPF days, the high solar radiation and air temperature during the daytime promote the emission of BVOCs (Ramasamy et al., 2016) and the formation of BSOA (Han et al., 2013, 2014). The relatively low RH values in the daytime might also be favorable for NPF, as suggested elsewhere (Hamed et al., 2011; Han et al., 2013). The O:C ratio of organics on average showed a daily minimum at the beginning of the accumulation of organics and increased steadily until the evening on NPF days (Figure 3b), whereas no evident variation of the ratio was observed on OTHER days (Figure 3f). This difference could be explained by the low O:C ratio of the newly formed BSOA at this site (Han et al., 2014). The diurnal variations of $N_{CCN,t}$ (Figures 3c and 3g) on NPF days were also stronger than those on OTHER days. Furthermore, the diurnal variations at high (0.42% and 0.80%) SS conditions were stronger than those at low (0.11% and 0.24%) SSs. From midnight to approximately noon, the $N_{CCN,t}$ values on NPF days were lower than those on OTHER days at all SS conditions. In the afternoon hours, while the $N_{CCN,t}$ values were at the same levels at 0.11%, 0.24%, and 0.42% SS, at 0.80% SS, the $N_{CCN,t}$ on NPF days was presumably substantially higher (p value: 0.12) than those on OTHER days at the time when the aerosol number concentration reached its maximum (Figure 2). The higher $N_{CCN,t}$ with a maximum on NPF days can be explained by the enhanced condensation of the locally formed fresh BSOA. Nevertheless, it may also indicate the contribution of NPF to increases in CCN, especially for small particle diameters.

4.2. Hygroscopicity of Aerosol Particles

The hygroscopicity parameters of ambient particles, κ_t, were derived from the calculated dry activation diameters (section 3.2). Figures 3d and 3h present the diurnal variations of κ_t on NPF and OTHER days, respectively. On NPF days, the decrease of κ_t coincided with the accumulation of organics (Figure 3a). Organic mass concentrations and κ_t reached their daily maximum and minimum, respectively, between 1200 and 1800 JST, while the mass concentration of inorganic components on average showed little variation in the daytime (Figure 2). In the evening, the weakening of the BSOA condensation and the dilution by the inflowing air masses presumably caused the decrease of organic mass concentration and led to the

Table 1
Statistics of κ_{org} and κ_{BSOA}

	κ_{org}[a]			κ_{BSOA}[b]		
SS (%)	Median	Mean	SD	Median	Mean	SD
0.11	0.18	0.22	0.13	0.11	0.12	0.05
0.23	0.18	0.20	0.13	0.08	0.10	0.05
0.42	0.17	0.18	0.13	−0.01	−0.03	0.07
0.80	0.17	0.19	0.13	0.07	0.06	0.04
All	0.18	0.19	0.13	0.09[c]	0.09[c]	0.05[c]

Note. SD = standard deviation; SS = supersaturation.
[a]Only data with $\varepsilon_{org} > 0.6$ were used. [b]See section 4.3 for details.
[c]Data at 0.42% SS were not included.

increase of κ_t. On OTHER days, the diurnal variation of κ_t was not clear, although a daily minimum was also found in the daytime. This is consistent with the lower accumulation of organics (Figure 3e) compared to that on NPF days.

The statistics of κ_t differentiated by the dry activation diameters are presented in Figure 4. The average κ_t on NPF days was smaller than that on OTHER days across the whole measured size range. On average, the measured κ_t increased with the increase in the particle diameter. The increase was obvious when particle diameter was greater than 100 nm. This is explained by the different chemical compositions of particles in the respective activation diameter ranges. Size-resolved chemical compositions (Figure S9) show that OA and sulfate, respectively, accounted for 67% and 12% of the mass of aerosol particles with $d_{act} < 100$ nm (corresponding to the d_{va} range of 44.4–199.7 nm), whereas OA and sulfate, respectively, accounted for 57% and 27% of the mass of aerosol particles with $d_{act} > 100$ nm (corresponding to the d_{va} range of 143.4–298.0 nm). The distinctive differences in the sulfate and OA mass fractions in sub-100-nm and super-100-nm activation diameter ranges can be explained by the different origins of the aerosol particles. Most super-100-nm particles probably originated from the inflowing air masses after long-range transport (Figure S6). Aerosol particles in air masses from the Asian continent and Japanese archipelago can be sulfate rich because of the anthropogenic activities that emit SO_2, a precursor of sulfate. Aerosol particles in the air masses from the North Pacific can also be sulfate rich, as reported by Mochida et al. (2011). Sulfur-containing air masses influenced by volcanic emissions could have also contributed to the sulfate in the observed aerosols. Additionally, the organics in the long-range transported aerosols are usually more hygroscopic than those in fresh aerosols due to their oxidation (Jimenez et al., 2009), which is consistent with the high hygroscopicity of the super-100-nm aerosols. Conversely, the sub-100-nm aerosols were more likely to be locally formed fresh aerosols, formed through the nucleation and condensational growth of organic and inorganic vapors. In this remote location, the formation of BSOA dominated the growth of these particles, as discussed in section 4.1 and indicated by Han et al. (2014).

The κ_t values from studies in other forest environments are also presented in Figure 4. It is shown that the particle hygroscopicity in the studied midlatitude forest was higher than those in other forests, especially in the sub-100-nm diameter range. This is likely caused by the lower aerosol organic mass fractions of this study compared with those of the other studies presented in Figure 4 (Paramonov et al., 2013). As stated above, organics accounted for 67% of the sub-100-nm aerosol mass in this study, while it accounted for

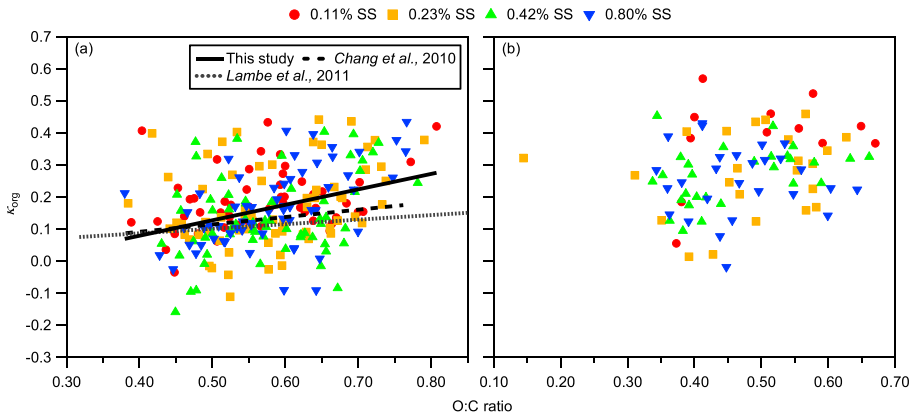

Figure 5. The κ_{org} versus the O:C ratio of the organics in the cases of (a) $m_{org} > 0.5$ μg/m^3 and (b) $m_{org} < 0.5$ μg/m^3. Only data with $\varepsilon_{org} > 0.6$ were used. The O:C ratios from Chang et al. (2010) and Lambe et al. (2011) were scaled by a factor of 1.27 to account for the difference in the method to calculate the O:C ratio (Canagaratna et al., 2015): The Improved-Ambient method and the Aitken-Ambient method were used in this study and former studies, respectively. SS = supersaturation.

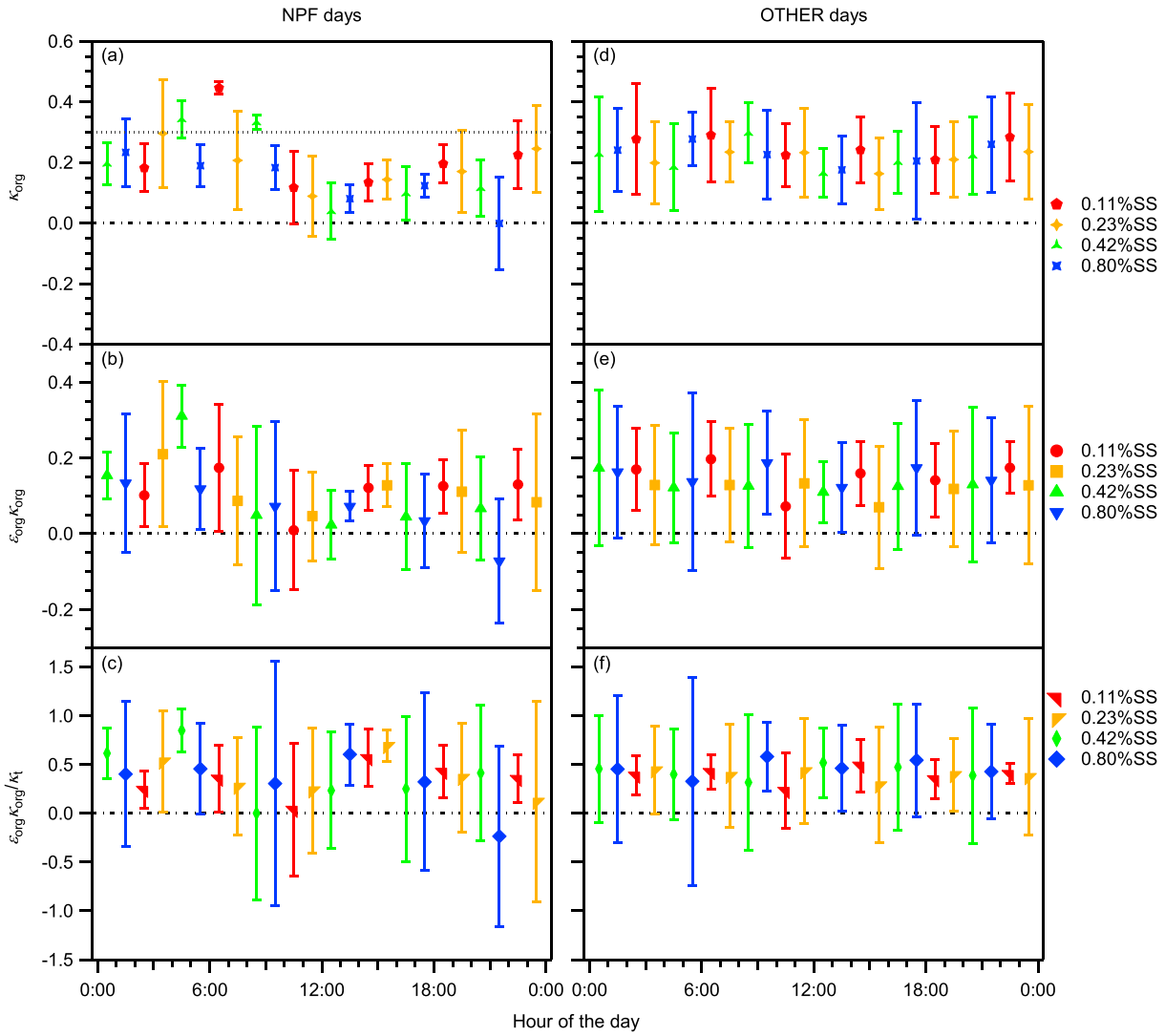

Figure 6. Diurnal variations of (a and d) κ_{org}, (b and e) $\varepsilon_{org}\kappa_{org}$, and (c and f) $\varepsilon_{org}\kappa_{org}/\kappa_t$ over the whole study period. Panels a, b, and c show NPF days, and panels d, e, and f show OTHER days. For panels a and d, only data with $\varepsilon_{org} > 0.6$ were used. The whiskers represent the standard deviations. NPF = new particle formation; SS = supersaturation.

approximately 90% and 80% of sub-100-nm aerosol masses in the Amazonian tropical forest (Gunthe et al., 2009) and the mountainous forest station in Colorado (Levin et al., 2014), respectively. Note that we did not find any information that supports this argument for the boreal forest. In the case of super-100-nm particles, the hygroscopicity of the studied aerosol particles was comparable to that of the particles in the boreal forest. In Wakayama, κ_t values that tended to be substantially lower than those observed in this study were previously observed for super-100-nm particles in the year of 2010 (Kawana et al., 2017). The lower OA mass fractions may have led to the higher κ_t in this study: The organic to sulfate mass ratio in the d_{va} range of 150–300 nm in this study was 2.1, whereas the ratio in 2010 was 7.8 (data from the work of Han et al., 2014). Compared with the Amazonian aerosols in the wet season, both the dry activation diameters and the hygroscopicity parameters of the studied aerosols showed much larger variations. The variations in the relative contributions of the long-range transported particles and locally formed particles in the forest in Wakayama may have resulted in stronger variations of κ_t.

4.3. Hygroscopicity of OA and BSOA

The statistics of κ_{org} under different SS conditions are summarized in Table 1. In this section, data points with $\varepsilon_{org} < 0.6$ were excluded for the analysis of κ_{org}, unless stated otherwise. This is because the uncertainty

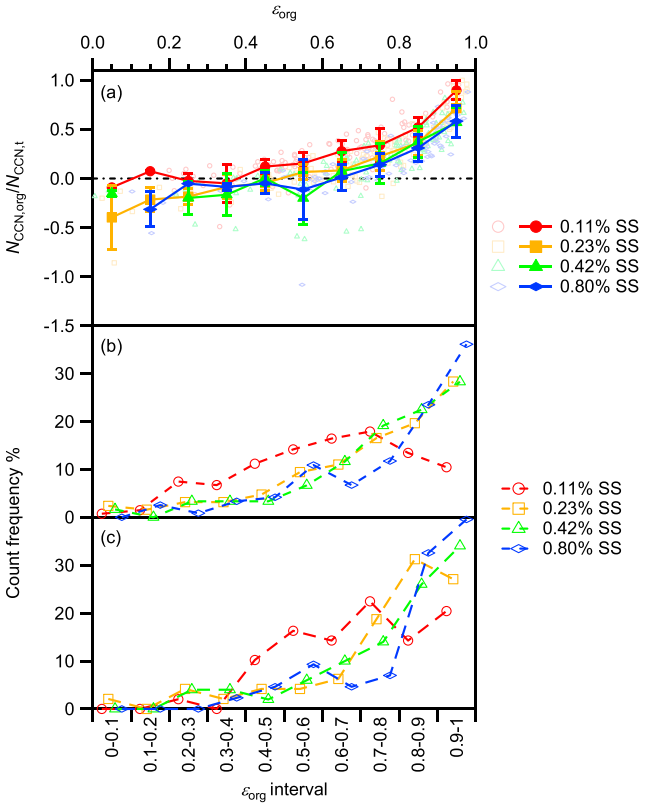

Figure 7. (a) $N_{CCN,org}/N_{CCN,t}$ versus ε_{org} over the whole study period, and the count frequencies (%) of ε_{org} in 0.1 intervals under the four different SS conditions for (b) the entire period and (c) the period from 1200 to 2000 JST. In panel a, the open markers represent individual data, and the filled markers and their whiskers represent the means and standard deviations of $N_{CCN,org}/N_{CCN,t}$ in respective 0.1 intervals. A whisker is not presented if only one data point is available. Note that the negative $N_{CCN,org}/N_{CCN,t}$ values were directly caused by the negative κ_{org} values (Figure S12). SS = supersaturation.

originating from the subtraction of the contribution of inorganic components is considered to be large when the organic volume fraction was low (Mei et al., 2013). Sensitivity analysis on the influence of the volume fraction of inorganics to κ_{org} is presented in S9. The results indicate that at $\varepsilon_{org} > 0.6$, κ_{org} and $\varepsilon_{org}\kappa_{org}$ are not sensitive to the 30% decrease of ε_{inorg}. The κ_{org} value at 0.11% SS was 0.22, which was, on average, larger than the values at higher SS conditions (p value: 0.06). When the SS was high (0.24%, 0.42%, and 0.80%), the κ_{org} values at the different SSs were very similar to each other: The averages were in the range of 0.18–0.20. The greater κ_{org} values of larger particles can be explained by its higher oxygenation as indicated by the fractions of m/z 44 in the mass spectrum of OA (f_{44}; Duplissy et al., 2011): In the d_{va} ranges that correspond to the activation diameters at 0.11%, 0.24%, and 0.42% SS, the mean f_{44} values were 0.089, 0.079, and 0.068, respectively. The κ_{org} values derived here are higher than the range of 0.06–0.16, that is, that based on the currently available data from field studies in forests (Cerully et al., 2011; Cerully et al., 2015; Dusek et al., 2010; Gunthe et al., 2009; Kawana et al., 2017; Levin et al., 2014; Pierce et al., 2012).

In Figure 5, the calculated κ_{org} was plotted against the O:C ratio of organics. Here only the data with $\varepsilon_{org} > 0.6$ are presented; the plots covering the whole ε_{org} range are presented in Figure S12. The κ_{org} values showed an increasing trend with an increasing O:C ratio when the measured mass concentration of OA (m_{org}) was greater than 0.5 μg/m^3 (Figure 5a). The correlation coefficient r of κ_{org} and the O:C ratio was 0.35 (p value: 1.12×10^{-8}). The regression line was $\kappa_{org} = 0.48$ (O:C) − 0.11. The data in Figure 5a are further plotted for NPF days and OTHER days (Figure S13). On NPF and OTHER days, the mean ± SD of the O:C ratio were 0.54 ± 0.07 and 0.62 ± 0.09, respectively. Thus, the low κ_{org} and O:C values could represent the properties of the OA in the newly formed particles, and the high κ_{org} and O:C could represent the properties of the OA in the long-range transported particles and/or in the locally formed but aged particles. The pattern of the variations of the O:C ratio on NPF days (Figure 3b) is consistent with the view that newly formed BSOA experienced the aging process, as also suggested by earlier observations (Han et al., 2014). The linear regressions of the κ_{org} against the O:C at a rural site in Ontario (Chang et al., 2010) and from laboratory-generated OA with precursors that represent atmospherically relevant biogenic and anthropogenic sources (Lambe et al., 2011) are also presented in Figure 5a. The slope of the regression line from this study is slightly larger than those for the rural site and the laboratory-generated OA. For $m_{org} < 0.5$ μg/m^3, no dependence of κ_{org} on the O:C ratio was observed (Figure 5b). The measurement uncertainty probably masked the dependence when the organic mass was small.

The diurnal variations of κ_{org} on NPF days and OTHER days are presented in Figures 6a and 6d, respectively. On both types of days, κ_{org} showed daily minima in the afternoon hours and reached maxima after midnight, although the variations on OTHER days were not as evident as those on NPF days. The strong condensation and/or in-particle formation of the fresh BSOA explain the daily minima, and the aging of the newly formed BSOA, as well as their replacement with regional aged aerosols, could explain the recovery of κ_{org} after midnight. On NPF days, κ_{org} was lower than those on OTHER days throughout the daytime until after midnight. While, on OTHER days, the mean daily minima of κ_{org} were larger than 0.15 for all SS conditions, on NPF days, except for at 0.11% SS, all the minima of κ_{org} values reached below 0.10 (0.09 for 0.24% SS during 1100–1200 JST, 0.04 for 0.42% SS during 1200–1300 JST, and 0.08 for 0.80% SS during 1300–1400 JST). This result indicates the low hygroscopicity of newly formed BSOA. Note that the large negative κ_{org} value appeared during 2100–2200 JST led to the negative mean κ_{org}. Measurement errors

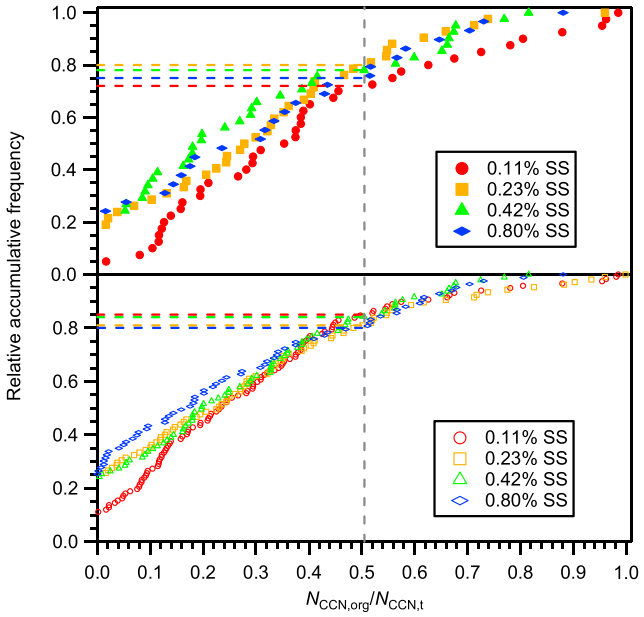

Figure 8. The relative accumulative frequency of $N_{CCN,org}/N_{CCN,t}$ (a) during 1200–2000 JST and (b) for the entire period. The vertical dashed lines indicate $N_{CCN,org}/N_{CCN,t}$ = 0.5. The relative accumulative frequencies at which $N_{CCN,org}/N_{CCN,t}$ reach >0.5 are presented as horizontal dashed lines with the same colors as the corresponding markers. SS = supersaturation.

may have caused the negative values. However, the possibility that the κ_{org}, which is defined by $(\kappa_t - \varepsilon_{inorg}\kappa_{inorg})/\kappa_{inorg}$, was really negative should not be ruled out, because the additivity assumption of water uptake (equation (5)) does not necessarily hold for some organic/inorganic mixtures (Chan & Chan, 2003; Vaishya et al., 2013).

The aerosol hygroscopicity that can be attributed to OA and the relative contributions of OA to water uptake were evaluated using the product of ε_{org} and κ_{org} and by the ratio of this product to κ_t ($\kappa_{org}\varepsilon_{org}/\kappa_t$). The means ± SD of $\kappa_{org}\varepsilon_{org}$ and $\kappa_{org}\varepsilon_{org}/\kappa_t$ during the study period were 0.12 ± 0.15 and 38% ± 57%, respectively. The diurnal variations of $\varepsilon_{org}\kappa_{org}$ on NPF days (Figure 6b) were characterized by daily minima around noon, similar to those of κ_{org}. After the minima, an afternoon maximum was observed, which corresponds to the afternoon maximum of ε_{org} (Figure S14a). Similar, but faint, diurnal variations of $\varepsilon_{org}\kappa_{org}$ were observed on OTHER days (Figure 6e), which is caused by the less distinct diurnal variations of both ε_{org} (Figure S14b) and κ_{org} (Figure 6d) than those on NPF days. Note that the above-stated diurnal variations of $\varepsilon_{org}\kappa_{org}$ were mainly present at low-SS conditions (0.11% and 0.24%); at high-SS conditions, which correspond to small particle activation diameters (d_{va} of 44.4–97.7 and 68.1–143.4 nm, Table S2), the measurement uncertainties in the chemical compositions probably masked the diurnal variations. The hourly mean values of $\varepsilon_{org}\kappa_{org}$, measured on a diurnal basis for both NPF and OTHER days, were in the range of 0–0.2, except during 0400–0500 JST on NPF days, when the hourly mean reached up to 0.3. The $\varepsilon_{org}\kappa_{org}/\kappa_t$ on NPF days (Figures 6c) presented a similar diurnal pattern as that of $\varepsilon_{org}\kappa_{org}$. On OTHER days, no obvious variations of $\varepsilon_{org}\kappa_{org}/\kappa_t$ were observed (Figure 6f).

To retrieve the hygroscopicity of the locally formed fresh BSOA (κ_{BSOA}), 5 days that meet the following criteria were selected (Figure 1): (1) The mean OA mass concentration between 1200 and 2000 JST was greater than two times that between 0600 and 0900 JST, and (2) the organic to sulfate mass ratio was high (>1) from 1200 to 2000 JST. Within the period of 1200–2000 JST on these five selected days, the periods when the fresh BSOA (section 3.2) were >1 μg/m^3 were further selected for the calculation of κ_{BSOA}. The obtained κ_{BSOA} is summarized in Table 1. The κ_{BSOA} of large particles activated under low-SS conditions was larger than that of small particles activated under high SS. The aging of organics during the growth of the particles can be expected to influence the size dependence of κ_{BSOA}. In the cases of 0.11% and 0.24% SS, κ_{BSOA} was, on average, 0.10–0.12, with an SD of 0.05. This value is same as the organic hygroscopicity parameter for particles with diameters of approximately 200 nm in the Amazonian rainforest during the wet season (Gunthe et al., 2009). At 0.80% SS, κ_{BSOA} was, on average, 0.06, with an SD of 0.04. In the case of 0.42% SS, the relative SD of the calculated κ_{BSOA} was large (2.9) and the mean κ_{BSOA} was negative, suggesting that the derivation attempt was unsuccessful. The overall mean ± SD of the κ_{BSOA} values obtained at 0.11%, 0.24%, and 0.80% SS was 0.09 ± 0.05, which is lower than the κ of the secondary OA from isoprene (0.20 ± 0.02) obtained through the positive matrix factorization and ZSR analysis of Cerully et al. (2015) but is within the ranges of the κ of the modeled BSOA (0.001–0.25) from several laboratory studies (Alfarra et al., 2013; Frosch et al., 2011, 2013; Kuwata et al., 2013; Lang-Yona et al., 2010; Massoli et al., 2010, and the references therein).

Table 2
The mean ± SD of $N_{CCN,org}$ and $N_{CCN,org}/N_{CCN,t}$

SS (%)	$N_{CCN,org}$ (particle/cm^3)	$N_{CCN,org}/N_{CCN,t}$ (%)
0.11	50 ± 54	26.7 ± 26.4
0.23	94 ± 145	23.5 ± 31.5
0.42	152 ± 321	20.0 ± 30.9
0.80	182 ± 498	19.4 ± 31.5

Note. SD = standard deviation.

4.4. Contribution of OA to CCN Number Concentrations

The relative contribution from the presence of OA to the CCN number concentrations ($N_{CCN,org}/N_{CCN,t}$) was assessed in view of the organic volume fraction of the aerosol particles (Figure 7). The contribution was found to be prominent (i.e., mean $N_{CCN,org}/N_{CCN,t}$ was greater than 30%) when ε_{org} was larger than approximately 70%. The contribution was especially large under low-SS conditions. When ε_{org} was greater

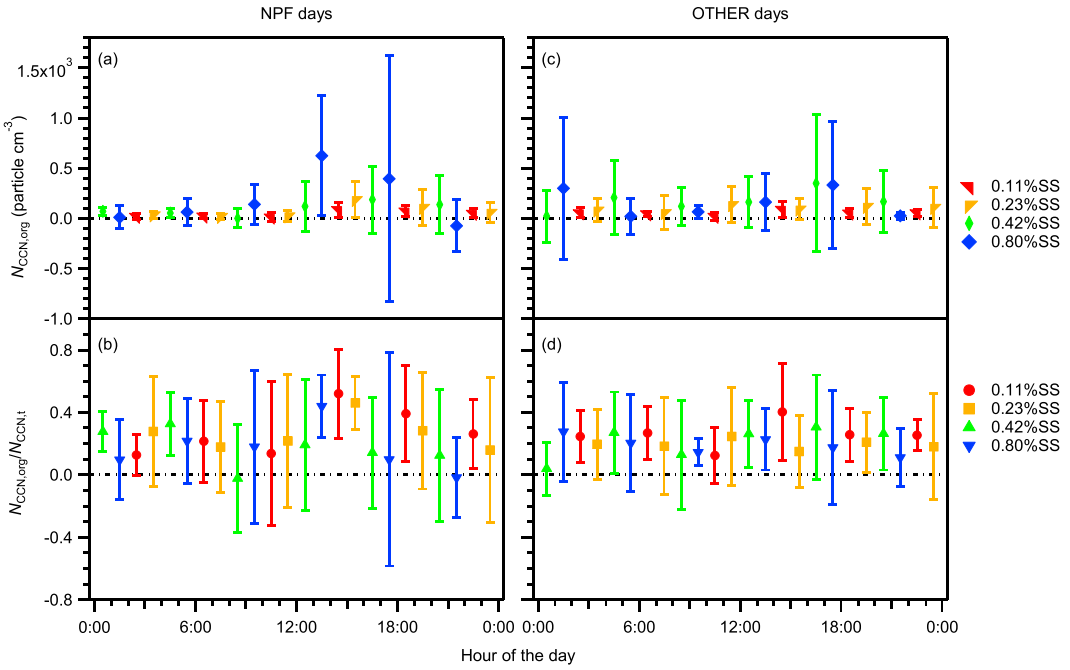

Figure 9. Diurnal variations of (a and c) $N_{CCN,org}$ and (b and d) $N_{CCN,org}/N_{CCN,t}$ over the whole study period. Panels a and b show NPF days, and panels c and d show OTHER days. The whiskers represent the standard deviations. NPF = new particle formation; SS = supersaturation.

than 70%, the mean ± SD of the contributions of the presence of OA to the CCN number concentrations at 0.80%, 0.42%, 0.24%, and 0.11% SS were 36% ± 23%, 35% ± 24%, 42% ± 25%, and 49% ± 24%, respectively. The occurrences of ε_{org} in each 0.1 interval over the entire study period and those collected during 1200–2000 JST are presented in Figures 7b and 7c, respectively. For the entire study period, the particles with $\varepsilon_{org} > 70\%$ accounted for 42%, 65%, 70%, and 71% of the observed particles in the activation diameter ranges of 0.11%, 0.24%, 0.42%, and 0.80% SS conditions, respectively. During 1200–2000 JST, the proportions were even more substantial: they were 57%, 77%, 74%, and 79%, respectively. The larger proportions of particles with high ε_{org} values observed in the afternoon hours than those during the entire study period is consistent with the higher mass concentration (Figure 2) and higher volume fraction (Figure S14) of organics observed in the afternoon, which was contributed by the formation of BSOA. The absolute number concentrations of CCNs that are contributed by the presence of organics ($N_{CCN,org}$, Figure S15) at $\varepsilon_{org} > 70\%$ were calculated to be 81, 161, 243, and 346 cm^{-3} at 0.11%, 0.24%, 0.42%, and 0.80% SS, respectively. These are quite substantial if compared with the super-30-nm particle concentration of approximately 200 cm^{-3} in the Amazonian forest during the wet season (Gunthe et al., 2009). Furthermore, the frequency of the occurrence of $N_{CCN,org}/N_{CCN,t}$ was analyzed to assess the contribution of organics to the CCN concentrations (Figure 8). The presence of organics increased the CCN concentration by more than 50% during 15–20% of the entire study period (Figure 8b). If only the data during 1200–2000 JST are considered (Figure 8a), this proportion increases to 20–28%, which is explained by the fact that higher proportions of particles have high ε_{org} during the afternoon (Figure 7).

The $N_{CCN,org}$ and $N_{CCN,org}/N_{CCN,t}$ calculated over the entire study period are summarized in Table 2. The mean values of $N_{CCN,org}$ and $N_{CCN,org}/N_{CCN,t}$ under the four SS conditions ranged from 50 to 182 particle/cm^3 and 27–19%, respectively. That increase of $N_{CCN,org}$ accompanying the increase of SS is explained by the high $dN_{CN}/d\log d_{dry}$ (Figure S16) and the high ε_{org} (Table S2) in the dry activation diameter ranges of the high-SS conditions. The $N_{CCN,org}/N_{CCN,t}$ presented a decreasing trend with increased SS; whereas $N_{CCN,org}$ at low SS was smaller than that at high SS on average, the $N_{CCN,t}$ at low SS was even smaller than that at high SS (section 4.1), which explains the trend of $N_{CCN,org}/N_{CCN,t}$. The large relative SDs of $N_{CCN,org}$ (ranging from 1.1 to 2.7) and $N_{CCN,org}/N_{CCN,t}$ (ranging from 1.0 to 1.6) are explained by the large temporal variations of the particle number-size distribution and chemical compositions (Figure 1).

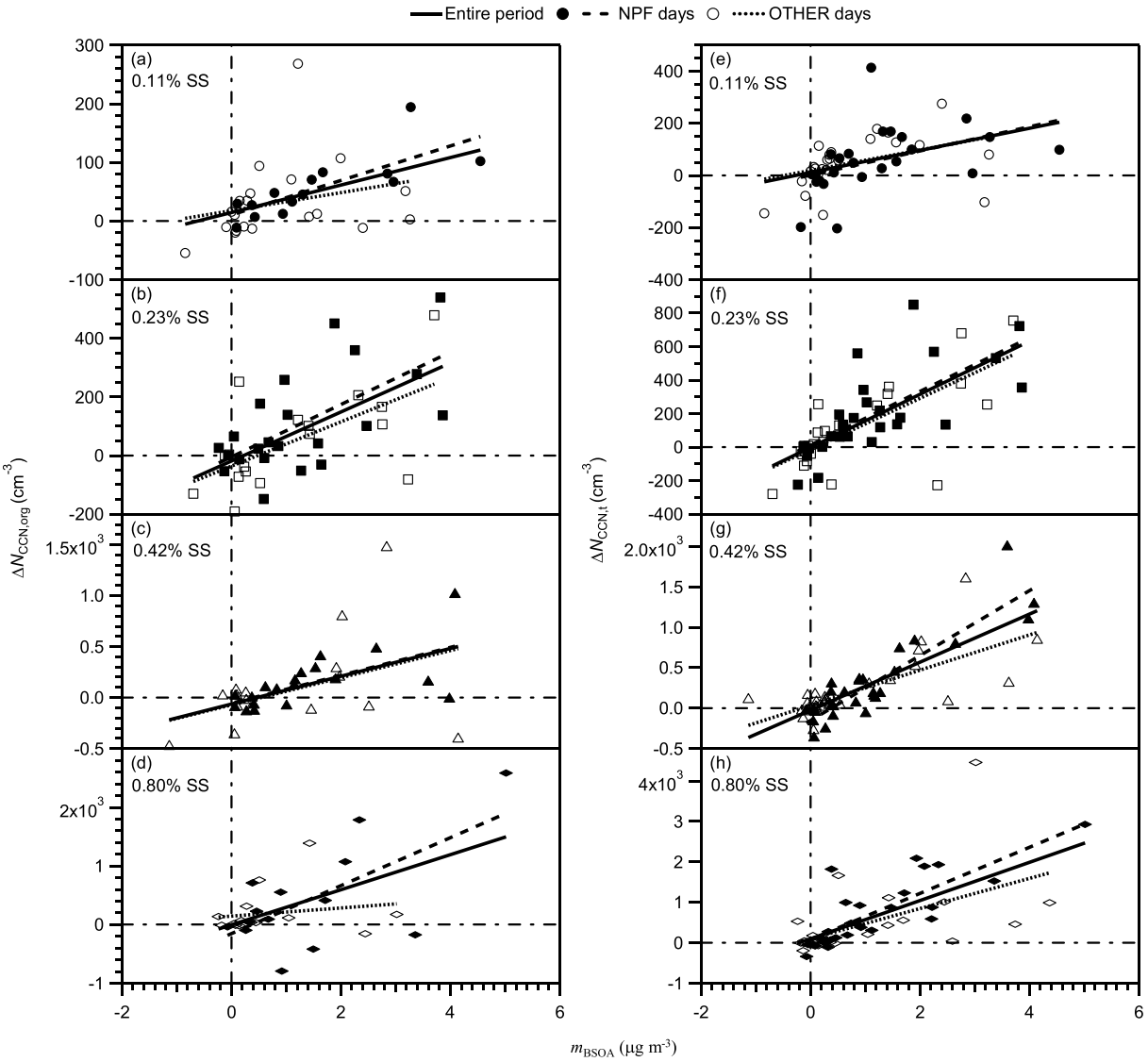

Figure 10. (a–d) The $\Delta N_{CCN,org}$ versus m_{BSOA} and (e–h) the $\Delta N_{CCN,t}$ versus m_{BSOA} at four different supersaturation (SS) conditions for the period of 1200–2000 JST. Filled markers: data on NPF days; open markers: data on OTHER days; solid lines: regression lines for the entire period; dashed lines: regression lines for NPF days; dotted lines: regression lines for OTHER days. NPF = new particle formation.

The diurnal variations of $N_{CCN,org}$ and $N_{CCN,org}/N_{CCN,t}$ on NPF and OTHER days are presented in Figure 9. On NPF days, the daily maxima of the $N_{CCN,org}$ were observed in the afternoon for all SS conditions, as were those of $N_{CCN,t}$ (Figure 3c). The diurnal patterns of $N_{CCN,org}/N_{CCN,t}$ on NPF days followed that of $\varepsilon_{org}\kappa_{org}/\kappa_t$ (Figure 6c): After the local minima appeared at the start of the accumulation of OA, the values increased towards the afternoon, and the daily maxima appeared in the afternoon for all the SS values except 0.42% SS, whose maximum appears at 0400–0500 JST, as that of $\varepsilon_{org}\kappa_{org}/\kappa_t$. On OTHER days, the diurnal variations of both $N_{CCN,org}$ and $N_{CCN,org}/N_{CCN,t}$ were not clear, which corresponds to the unclear diurnal variations of $N_{CCN,t}$ (Figure 3g) and $\varepsilon_{org}\kappa_{org}/\kappa_t$ (Figure 6f). Besides the CCN number concentration and the hygroscopicity of OA, the diurnal variations of the size distributions of the aerosol particles may also have affected the diurnal variations of $N_{CCN,org}$ and $N_{CCN,org}/N_{CCN,t}$ but were not discussed in this study.

To assess the contribution of BSOA to the CCN number concentration, $\Delta N_{CCN,org}$ and $\Delta N_{CCN,t}$, that is, the difference of the obtained $N_{CCN,org}$ and $N_{CCN,t}$ from their individual background values (see section 3.3), during 1200–2000 JST were plotted against the mass concentrations of the locally formed fresh BSOA (m_{BSOA}; Figure 10). Note that the diurnal variations of the mass concentrations of the main chemical components

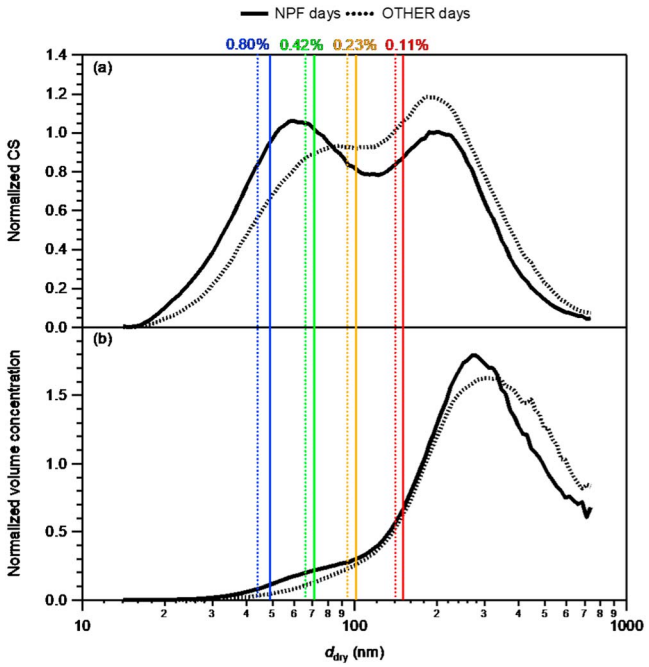

Figure 11. Averages of the normalized size distributions of (a) the condensation sink (CS) and (b) the volume concentration of the aerosols across the measured size range for (solid line) NPF and (dotted line) OTHER days over the whole study period. The mean activation diameters under the different supersaturation (SS) conditions are presented as vertical lines. The percentages above the vertical lines are the corresponding SS values. NPF = new particle formation.

of the aerosols in the studied 44.4- to 298.0-nm aerosol diameter range (Figure S17) indicate that OA was the main contributor to the increase in the solute mass that increased the CCN number concentration ($N_{CCN,t}$). Thus, $\Delta N_{CCN,t}$ was also adopted to analyze the contribution of BSOA to the CCN number concentrations. Linear regressions of $\Delta N_{CCN,org}$ ($\Delta N_{CCN,t}$) and m_{BSOA} were performed for the entire study period, NPF days, and OTHER days. The resulting correlation coefficients and slopes are presented in Table S6. Over the entire study period, the correlation coefficients r of $\Delta N_{CCN,org}$ and m_{BSOA} were in the range of 0.47–0.62 and that of $\Delta N_{CCN,t}$ and m_{BSOA} were in the range of 0.43–0.81. The positive correlations suggest the contribution of the formation of BSOA to the CCN number concentrations. The slopes of the linear regression between $\Delta N_{CCN,org}$ ($\Delta N_{CCN,t}$) and m_{BSOA} were 23 (42), 84 (159), 136 (297), and 299 (471) g^{-1} at the activation diameters of 145 ± 18, 97 ± 13, 68 ± 9, and 46 ± 6 nm, respectively. Tunved et al. (2008) estimated the potential CCN concentration (assuming d_{act} = 80 nm) of 197 cm^{-3} with a BSOA mass concentration of 0.85 $\mu g/m^3$ for the natural aerosols in the boreal forest, which results in an $\Delta N_{CCN,org}$ to m_{BSOA} ratio of 232 g^{-1}. This is about twice the value of $\Delta N_{CCN,org}$ versus m_{BSOA} but is close to the value of $\Delta N_{CCN,t}$ versus m_{BSOA}, for a similar size range to that of this study.

Furthermore, to evaluate the effects of the NPF on the contribution of the fresh BSOA to CCN number concentrations, the slopes of the linear regressions of $\Delta N_{CCN,org}$ ($\Delta N_{CCN,t}$) against m_{BSOA} for the NPF and OTHER days were compared, and the significance of the difference was represented by the p value of the two-sided t test (details of the method of comparison are presented in Text S10, and the results are presented in Table S6). At 0.11% and 0.24% SS, there were no significant differences in the slopes of the linear regressions of both $\Delta N_{CCN,org}$ against m_{BSOA} and $\Delta N_{CCN,t}$ against m_{BSOA} between NPF and OTHER days. At 0.42% SS, although the difference of $\Delta N_{CCN,org}$ against m_{BSOA} was not evident, the difference of $\Delta N_{CCN,t}$ against m_{BSOA} between NPF and OTHER days was significant, with a p value of 0.001. At 0.80% SS, both the differences of the $\Delta N_{CCN,org}$ against m_{BSOA} and $\Delta N_{CCN,t}$ against m_{BSOA} between NPF and OTHER days were significant, with p values of 0.094 and 0.193, respectively. Note that the correlation between $\Delta N_{CCN,org}$ and m_{BSOA} at 0.80% SS for the OTHER days was poor (r = 0.17), which may be caused by the low CCN number concentration or possible measurement errors.

The retrieved contributions of the locally formed fresh BSOA to the CCN number concentrations under the different SS conditions are assessed by the size distributions of the BSOA. The BSOA size distribution is determined by the size distribution of condensation sink (CS) for the case of irreversible condensation when the condensed products are of extremely low volatility or by the mass-size distribution of organics if the condensed products are semivolatile and in equilibrium with the gas phase (Odum et al., 1996). Laboratory experiments indicate that BSOA can be of high or low volatility (Jimenez et al., 2009). The average of size distributions of normalized CS and aerosol volume concentrations (a rough estimate of the organic mass concentration) were derived for NPF and OTHER days (Figure 11). At 0.11% and 0.24% SS, the normalized CS on NPF days was slightly lower (−14% and −13%, respectively) than that on OTHER days, and the particle volume concentration was slightly higher (29% and 31%, respectively). The similarities of both normalized CS and particle volume concentrations between NPF and OTHER days indicate that the condensation of BSOA can be similar on NPF and OTHER days, explaining why the results of the linear regressions of $\Delta N_{CCN,org}$ against m_{BSOA} and $\Delta N_{CCN,t}$ against m_{BSOA} between NPF and OTHER days do not show significant differences (Figures 10a, 10b, 10e, and 10f, and Table S6). At 0.42% and 0.80% SS, both the normalized CS and particle volume concentrations around the activation diameters on the NPF days were larger than those on the OTHER days: The normalized CS on NPF days were 17% and 67% greater than that on OTHER days for 0.42% SS and 0.80% SS, respectively; the normalized particle volume concentrations on NPF days were 1.0

and 2.4 times higher than that on OTHER days for 0.42% SS and 0.80% SS, respectively. Thus, significantly larger slopes of the regression lines of $\Delta N_{CCN,org}$ ($\Delta N_{CCN,t}$) against m_{BSOA} for NPF than those on OTHER days are expected. The comparisons of $\Delta N_{CCN,t}$ against m_{BSOA} at 0.80% and 0.42% SS and $\Delta N_{CCN,org}$ against m_{BSOA} at 0.80% SS are consistent with this result; the difference of the slopes of $\Delta N_{CCN,org}$ against m_{BSOA} at 0.42% SS was insignificant. From the above discussions, we may conclude that NPF enhances the contributions of the locally formed fresh BSOA to the CCN number concentrations at high-SS conditions (0.42% and 0.80% SS). Given that this analysis is based on limited data, further studies of longer time periods are required to fully prove this enhancement.

5. Summary and Conclusions

The size-resolved CCN fractions, chemical compositions, and number concentrations of the atmospheric aerosols were measured for a midlatitude forest facing the western North Pacific in Japan during the summer of 2014. The number concentrations of the aerosols were 1,238 ± 1,468 cm^{-3}; those of CCN were 166 ± 133, 291 ± 265, 487 ± 556, and 740 ± 852 cm^{-3} at 0.11%, 0.24%, 0.42%, and 0.80% SS, respectively. While the mass concentration of sulfate was comparable to that of OA in the submicrometer diameter range, OA dominated the aerosol mass in the vacuum aerodynamic diameter range of 44.4–298.0 nm, which corresponds to the CCN activation diameters under the studied SS conditions of 0.11–0.80%. The particle hygroscopicity (κ_t) increased with increases of particle diameters, and it was higher than those measured in other forests for the sub-100-nm particle diameter range. The temporal variations of the mass and number concentrations and the hygroscopicity of the ambient aerosols were influenced by the inflowing air masses. The daily maxima of the $N_{CCN,t}$ and m_{org} values and the daily minima of κ_t were observed during the afternoon. NPF events were identified in 15 out of the 32 observation days. Diurnal variations of $N_{CCN,t}$, m_{org}, and κ_t were more evident on NPF days than those on the OTHER days.

The hygroscopicity of OA and BSOA and their contributions to CCN were characterized. κ_{org} increased with increases in the corresponding activation diameters and ranged from 0.18 to 0.22. The daily minimum κ_{org} was observed around noon. A positive relationship between κ_{org} and the O:C ratio of organics was derived: k_{org} = 0.48 (O:C) − 0.11, resulting in a correlation coefficient of 0.35. The lower sides of κ_{org} and the O:C ratio could represent the properties of OA in newly formed particles, while the higher sides of κ_{org} and the O:C ratio could represent the properties of OA in particles in long-range transported air masses or locally formed but aged particles. The hygroscopicity parameter of freshly formed BSOA (κ_{BSOA}) was estimated to be 0.09 ± 0.05. The aerosol hygroscopicity that can be attributed to OA and the relative contribution of OA to the water uptake were 0.12 ± 0.15 and 38% ± 57%, respectively. The contribution of OA to the CCN number concentration ($N_{CCN,org}$) was assessed by subtracting the CCN concentration of the hypothetical inorganic aerosols ($N_{CCN,inorg}$) from the ambient CCN concentration ($N_{CCN,t}$). $N_{CCN,org}$ was considerably large when ε_{org} was greater than 70%. The $N_{CCN,org}$ overwhelmed $N_{CCN,inorg}$ during 15–20% of the study period. In the period of 1200–2000 JST, the proportion increased to 20–28%, which is explained by the increase in the organic volume fraction during the afternoon hours. On average, $N_{CCN,org}$ ranged 50–182 cm^{-3} and accounted for 27–19% of the ambient CCN number concentrations at the studied SS conditions. The condensation of BSOA increased the CCN number concentration via its supply of extra solute masses. The increases of the CCN number concentrations per 1 $\mu g/m^3$ BSOA at 0.11%, 0.24%, 0.42%, and 0.80% SS were, on average, 23, 84, 136, and 299 cm^{-3}, respectively. Statistical analysis implies that NPF events enhance the contribution of BSOA to the CCN number concentrations at high-SS conditions (0.42% and 0.80%) in this midlatitude forest, but further studies covering longer time periods with larger data sets are required to draw this conclusion.

This study demonstrated that the organic and biogenic secondary organic fractions of aerosol particles are important to the hygroscopicity and CCN number concentrations of aerosols in the midlatitude forests. However, several issues are worth further studying to make these results more applicable and/or robust. First, although a positive relationship between κ_{org} and the O:C ratio was observed in this study, as reported from some previous studies, the correlation was weak and an applicable and accurate method to represent κ_{org} in modeling studies is still needed. Second, a more accurate estimation of locally formed fresh BSOA, such as a method using positive matrix factorization analysis of the OA components, is a subject for future studies. Third, the efficiency of the contribution of BSOA to the CCN number concentration

and the influence of NPFs on it are worth further studying, in order to understand the role of BSOA in biosphere-aerosol-climate interactions. Because the contribution of BSOA to CCN number concentration depends on environmental conditions, further studies should be performed in both the forest of this study and other forest environments.

Acknowledgments
We thank the faculty and staff of the Wakayama Forest Research Station, Field Science Education and Research Center of Kyoto University, Japan, for the use of the study site and for the meteorological data. We thank Tomomi Takeuchi for the help in the analysis of filter samples. We appreciate the authors of Han et al. (2014) for providing the AMS data for the year 2010. We acknowledge Kazuma Aoki for the use of the 1λ-PSAP instrument and Yoshizumi Kajii, Akira Ida, and other members who have attended the field study for their help and discussions during the observations. We acknowledge the NOAA Air Resources Laboratory (ARL) for providing the HYSPLIT model (http://www.ready.noaa.gov). This study was supported in part by JSPS KAKENHI grants JP26281007 (recipients: T. Nakayama, Y. Miyazaki, and M. Mochida), JP25740008 (recipient: K. Adachi), and JP16K16188 (recipient: K. Adachi). All final derived data supporting the findings of this study are available in the article and its supporting information file.

References

Adachi, K., Moteki, N., Kondo, Y., & Igarashi, Y. (2016). Mixing states of light-absorbing particles measured using a transmission electron microscope and a single-particle soot photometer in Tokyo, Japan. *Journal of Geophysical Research: Atmospheres*, *121*, 9153–9164. https://doi.org/10.1002/2016JD025153

Alfarra, M. R., Good, N., Wyche, K. P., Hamilton, J. F., Monks, P. S., Lewis, A. C., & McFiggans, G. (2013). Water uptake is independent of the inferred composition of secondary aerosols derived from multiple biogenic VOCs. *Atmospheric Chemistry and Physics*, *13*(23), 11,769–11,789. https://doi.org/10.5194/acp-13-11769-2013

Bianchi, F., Tröstl, J., Junninen, H., Frege, C., Henne, S., Hoyle, C. R., et al. (2016). New particle formation in the free troposphere: A question of chemistry and timing. *Science*, *352*(6289), 1109–1112. https://doi.org/10.1126/science.aad5456

Canagaratna, M. R., Jimenez, J. L., Kroll, J. H., Chen, Q., Kessler, S. H., Massoli, P., et al. (2015). Elemental ratio measurements of organic compounds using aerosol mass spectrometry: Characterization, improved calibration, and implications. *Atmospheric Chemistry and Physics*, *15*(1), 253–272. https://doi.org/10.5194/acp-15-253-2015

Carslaw, K. S., Boucher, O., Spracklen, D. V., Mann, G. W., Rae, J. G. L., Woodward, S., & Kulmala, M. (2010). A review of natural aerosol interactions and feedbacks within the Earth system. *Atmospheric Chemistry and Physics*, *10*(4), 1701–1737. https://doi.org/10.5194/acp-10-1701-2010

Cerully, K. M., Bougiatioti, A., Hite Jr, J. R., Guo, H., Xu, L., Ng, N. L., et al. (2015). On the link between hygroscopicity, volatility, and oxidation state of ambient and water-soluble aerosols in the southeastern United States. *Atmospheric Chemistry and Physics*, *15*(15), 8679–8694. https://doi.org/10.5194/acp-15-8679-2015

Cerully, K. M., Raatikainen, T., Lance, S., Tkacik, D., Tiitta, P., Petäjä, T., et al. (2011). Aerosol hygroscopicity and CCN activation kinetics in a boreal forest environment during the 2007 EUCAARI campaign. *Atmospheric Chemistry and Physics*, *11*(23), 12,369–12,386. https://doi.org/10.5194/acp-11-12369-2011

Chan, M. N., & Chan, C. K. (2003). Hygroscopic properties of two model humic-like substances and their mixtures with inorganics of atmospheric importance. *Environmental Science & Technology*, *37*(22), 5109–5115. https://doi.org/10.1021/es034272o

Chang, R. Y. W., Slowik, J. G., Shantz, N. C., Vlasenko, A., Liggio, J., Sjostedt, S. J., et al. (2010). The hygroscopicity parameter (κ) of ambient organic aerosol at a field site subject to biogenic and anthropogenic influences: Relationship to degree of aerosol oxidation. *Atmospheric Chemistry and Physics*, *10*(11), 5047–5064. https://doi.org/10.5194/acp-10-5047-2010

Clegg, S. L., Brimblecombe, P., & Wexler, A. S. (1998). Thermodynamic model of the system H^+–NH_4^+–SO_4^{2-}–NO_3^-–H_2O at tropospheric temperatures. *The Journal of Physical Chemistry A*, *102*(12), 2137–2154. https://doi.org/10.1021/jp973042r

DeCarlo, P. F., Kimmel, J. R., Trimborn, A., Northway, M. J., Jayne, J. T., Aiken, A. C., et al. (2006). Field-deployable, high-resolution, time-of-flight aerosol mass spectrometer. *Analytical Chemistry*, *78*(24), 8281–8289. https://doi.org/10.1021/ac061249n

Draxler, R. R., & Hess, G. D. (1998). An overview of the HYSPLIT_4 modelling system for trajectories, dispersion on and deposition. *Australian Meteorological Magazine*, *47*, 295–308.

Draxler, R. R., Hess, G. D., Laboratory, A. R., & Laboratories, E. R. (1997). *Description of the HYSPLIT-4 modeling system* (NOAA technical memorandum ERL ARL). Silver Spring, MD: National Oceanic and Atmospheric Administration.

Duplissy, J., DeCarlo, P. F., Dommen, J., Alfarra, M. R., Metzger, A., Barmpadimos, I., et al. (2011). Relating hygroscopicity and composition of organic aerosol particulate matter. *Atmospheric Chemistry and Physics*, *11*, 1155–1165. https://doi.org/10.5194/acp-11-1155-2011

Dusek, U., Frank, G. P., Curtius, J., Drewnick, F., Schneider, J., Kürten, A., et al. (2010). Enhanced organic mass fraction and decreased hygroscopicity of cloud condensation nuclei (CCN) during new particle formation events. *Geophysical Research Letters*, *37*, L03804. https://doi.org/10.1029/2009GL040930

Engelhart, G. J., Asa-Awuku, A., Nenes, A., & Pandis, S. N. (2008). CCN activity and droplet growth kinetics of fresh and aged monoterpene secondary organic aerosol. *Atmospheric Chemistry and Physics*, *8*(14), 3937–3949. https://doi.org/10.5194/acp-8-3937-2008

Farmer, D. K., Cappa, C. D., & Kreidenweis, S. M. (2015). Atmospheric processes and their controlling influence on cloud condensation nuclei activity. *Chemical Reviews*, *115*(10), 4199–4217. https://doi.org/10.1021/cr5006292

Frosch, M., Bilde, M., DeCarlo, P. F., Jurányi, Z., Tritscher, T., Dommen, J., et al. (2011). Relating cloud condensation nuclei activity and oxidation level of α-pinene secondary organic aerosols. *Journal of Geophysical Research*, *116*, D22212. https://doi.org/10.1029/2011JD016401

Frosch, M., Bilde, M., Nenes, A., Praplan, A. P., Jurányi, Z., Dommen, J., et al. (2013). CCN activity and volatility of β-caryophyllene secondary organic aerosol. *Atmospheric Chemistry and Physics*, *13*(4), 2283–2297. https://doi.org/10.5194/acp-13-2283-2013

Gunthe, S. S., King, S. M., Rose, D., Chen, Q., Roldin, P., Farmer, D. K., et al. (2009). Cloud condensation nuclei in pristine tropical rainforest air of Amazonia: Size-resolved measurements and modeling of atmospheric aerosol composition and CCN activity. *Atmospheric Chemistry and Physics*, *9*(19), 7551–7575. https://doi.org/10.5194/acp-9-7551-2009

Guo, X., Nakayama, T., Yamada, H., Inomata, S., Tonokura, K., & Matsumi, Y. (2014). Measurement of the light absorbing properties of diesel exhaust particles using a three-wavelength photoacoustic spectrometer. *Atmospheric Environment*, *94*, 428–437. https://doi.org/10.1016/j.atmosenv.2014.05.042

Hallquist, M., Wenger, J. C., Baltensperger, U., Rudich, Y., Simpson, D., Claeys, M., et al. (2009). The formation, properties and impact of secondary organic aerosol: Current and emerging issues. *Atmospheric Chemistry and Physics*, *9*(14), 5155–5236. https://doi.org/10.5194/acp-9-5155-2009

Hamed, A., Korhonen, H., Sihto, S.-L., Joutsensaari, J., Järvinen, H., Petäjä, T., et al. (2011). The role of relative humidity in continental new particle formation. *Journal of Geophysical Research*, *116*, D03202. https://doi.org/10.1029/2010JD014186

Han, Y., Iwamoto, Y., Nakayama, T., Kawamura, K., Hussein, T., & Mochida, M. (2013). Observation of new particle formation over a mid-latitude forest facing the North Pacific. *Atmospheric Environment*, *64*, 77–84. https://doi.org/10.1016/j.atmosenv.2012.09.036

Han, Y., Iwamoto, Y., Nakayama, T., Kawamura, K., & Mochida, M. (2014). Formation and evolution of biogenic secondary organic aerosol over a forest site in Japan. *Journal of Geophysical Research: Atmospheres*, *119*, 259–273. https://doi.org/10.1002/2013JD020390

Hussein, T., Dal Maso, M., Petaja, T., Koponen, I. K., Paatero, P., Aalto, P. P., et al. (2005). Evaluation of an automatic algorithm for fitting the particle number size distributions. *Boreal Environment Research*, *10*, 337–355.

Irwin, M., Robinson, N., Allan, J. D., Coe, H., & McFiggans, G. (2011). Size-resolved aerosol water uptake and cloud condensation nuclei measurements as measured above a Southeast Asian rainforest during OP3. *Atmospheric Chemistry and Physics*, *11*(21), 11,157–11,174. https://doi.org/10.5194/acp-11-11157-2011

Jimenez, J. L., Canagaratna, M. R., Donahue, N. M., Prevot, A. S. H., Zhang, Q., Kroll, J. H., et al. (2009). Evolution of organic aerosols in the atmosphere. *Science*, *326*(5959), 1525–1529. https://doi.org/10.1126/science.1180353

Kawana, K., Kuba, N., & Mochida, M. (2014). Assessment of cloud condensation nucleus activation of urban aerosol particles with different hygroscopicity and the application to the cloud parcel model. *Journal of Geophysical Research: Atmospheres*, *119*, 3352–3371. https://doi.org/10.1002/2013JD020827

Kawana, K., Nakayama, T., Kuba, N., & Mochida, M. (2017). Hygroscopicity and cloud condensation nucleus activity of forest aerosol particles during summer in Wakayama, Japan. *Journal of Geophysical Research: Atmospheres*, *122*, 3042–3064. https://doi.org/10.1002/2016JD025660

Kirkby, J., Duplissy, J., Sengupta, K., Frege, C., Gordon, H., Williamson, C., et al. (2016). Ion-induced nucleation of pure biogenic particles. *Nature*, *533*(7604), 521–526. https://doi.org/10.1038/nature17953

Kondo, Y., Sahu, L., Kuwata, M., Miyazaki, Y., Takegawa, N., Moteki, N., et al. (2009). Stabilization of the mass absorption cross section of black carbon for filter-based absorption photometry by the use of a heated inlet. *Aerosol Science and Technology*, *43*(8), 741–756. https://doi.org/10.1080/02786820902889879

Kuwata, M., Shao, W., Lebouteiller, R., & Martin, S. T. (2013). Classifying organic materials by oxygen-to-carbon elemental ratio to predict the activation regime of cloud condensation nuclei (CCN). *Atmospheric Chemistry and Physics*, *13*(10), 5309–5324. https://doi.org/10.5194/acp-13-5309-2013

Kuwata, M., Zorn, S. R., & Martin, S. T. (2012). Using elemental ratios to predict the density of organic material composed of carbon, hydrogen, and oxygen. *Environmental Science & Technology*, *46*(2), 787–794. https://doi.org/10.1021/es202525q

Kyoto University (2015). Wakayama Forest Research Station, Field Science Education and Research Center, Kyoto University, Japan. Retrieved from http://fserc.kyoto-u.ac.jp/wp/wakayama/topics/weather-data/2014

Kyoto University (2016). Kenkyurin · Shikenchi Joho 2010. In: Sections of Forest Station Management and Field Station Management, Field Science Education and Research Center, Kyoto University, Japan (in Japanese).

Lambe, A. T., Onasch, T. B., Massoli, P., Croasdale, D. R., Wright, J. P., Ahern, A. T., et al. (2011). Laboratory studies of the chemical composition and cloud condensation nuclei (CCN) activity of secondary organic aerosol (SOA) and oxidized primary organic aerosol (OPOA). *Atmospheric Chemistry and Physics*, *11*(17), 8913–8928. https://doi.org/10.5194/acp-11-8913-2011

Lang-Yona, N., Rudich, Y., Mentel, T. F., Bohne, A., Buchholz, A., Kiendler-Scharr, A., et al. (2010). The chemical and microphysical properties of secondary organic aerosols from holm oak emissions. *Atmospheric Chemistry and Physics*, *10*(15), 7253–7265. https://doi.org/10.5194/acp-10-7253-2010

Levin, E. J. T., Prenni, A. J., Palm, B. B., Day, D. A., Campuzano-Jost, P., Winkler, P. M., et al. (2014). Size-resolved aerosol composition and its link to hygroscopicity at a forested site in Colorado. *Atmospheric Chemistry and Physics*, *14*(5), 2657–2667. https://doi.org/10.5194/acp-14-2657-2014

Levin, E. J. T., Prenni, A. J., Petters, M. D., Kreidenweis, S. M., Sullivan, R. C., Atwood, S. A., et al. (2012). An annual cycle of size-resolved aerosol hygroscopicity at a forested site in Colorado. *Journal of Geophysical Research*, *117*, D06201. https://doi.org/10.1029/2011JD016854

Massoli, P., Lambe, A. T., Ahern, A. T., Williams, L. R., Ehn, M., Mikkila, J., et al. (2010). Relationship between aerosol oxidation level and hygroscopic properties of laboratory generated secondary organic aerosol (SOA) particles. *Geophysical Research Letters*, *37*, L24801. https://doi.org/10.1029/2010GL045258

Mei, F., Hayes, P. L., Ortega, A., Taylor, J. W., Allan, J. D., Gilman, J., et al. (2013). Droplet activation properties of organic aerosols observed at an urban site during CalNex-LA. *Journal of Geophysical Research: Atmospheres*, *118*, 2903–2917. https://doi.org/10.1002/jgrd.50285

Merikanto, J., Spracklen, D. V., Mann, G. W., Pickering, S. J., & Carslaw, K. S. (2009). Impact of nucleation on global CCN. *Atmospheric Chemistry and Physics*, *9*(21), 8601–8616. https://doi.org/10.5194/acp-9-8601-2009

Middlebrook, A. M., Bahreini, R., Jimenez, J. L., & Canagaratna, M. R. (2012). Evaluation of composition-dependent collection efficiencies for the aerodyne aerosol mass spectrometer using field data. *Aerosol Science and Technology*, *46*(3), 258–271. https://doi.org/10.1080/02786826.2011.620041

Mochida, M., Nishita-Hara, C., Furutani, H., Miyazaki, Y., Jung, J., Kawamura, K., & Uematsu, M. (2011). Hygroscopicity and cloud condensation nucleus activity of marine aerosol particles over the western North Pacific. *Journal of Geophysical Research*, *116*, D06204. https://doi.org/10.1029/2010JD014759

Mochida, M., Nishita-Hara, C., Kitamori, Y., Aggarwal, S. G., Kawamura, K., Miura, K., & Takami, A. (2010). Size-segregated measurements of cloud condensation nucleus activity and hygroscopic growth for aerosols at Cape Hedo, Japan, in spring 2008. *Journal of Geophysical Research*, *115*, D21207. https://doi.org/10.1029/2009JD013216

Müller, A., Miyazaki, Y., Tachibana, E., Kawamura, K., & Hiura, T. (2017). Evidence of a reduction in cloud condensation nuclei activity of water-soluble aerosols caused by biogenic emissions in a cool-temperate forest. *Scientific Reports*, *7*(1), 8452. https://doi.org/10.1038/s41598-017-08112-9

Odum, J. R., Hoffmann, T., Bowman, F., Collins, D., Flagan, R. C., & Seinfeld, J. H. (1996). Gas/particle partitioning and secondary organic aerosol yields. *Environmental Science & Technology*, *30*, 2580–2585. https://doi.org/10.1021/es950943+

Okumura, M. (2009). Estimation of volatile organic compound emissions from forest vegetation, PhD thesis, Graduate School of Energy Science, Kyoto Univ., Kyoto, Japan.

Paasonen, P., Asmi, A., Petaja, T., Kajos, M. K., Aijala, M., Junninen, H., et al. (2013). Warming-induced increase in aerosol number concentration likely to moderate climate change. *Nature Geoscience*, *6*(6), 438–442. https://doi.org/10.1038/ngeo1800

Paramonov, M., Aalto, P. P., Asmi, A., Prisle, N., Kerminen, V. M., Kulmala, M., & Petäjä, T. (2013). The analysis of size-segregated cloud condensation nuclei counter (CCNC) data and its implications for cloud droplet activation. *Atmospheric Chemistry and Physics*, *13*(20), 10,285–10,301. https://doi.org/10.5194/acp-13-10285-2013

Park, K., Kittelson, D., Zachariah, M., & McMurry, P. (2004). Measurement of inherent material density of nanoparticle agglomerates. *Journal of Nanoparticle Research*, *6*(2/3), 267–272. https://doi.org/10.1023/B:NANO.0000034657.71309.e6

Petters, M. D., & Kreidenweis, S. M. (2007). A single parameter representation of hygroscopic growth and cloud condensation nucleus activity. *Atmospheric Chemistry and Physics*, *7*(8), 1961–1971. https://doi.org/10.5194/acp-7-1961-2007

Pierce, J. R., Leaitch, W. R., Liggio, J., Westervelt, D. M., Wainwright, C. D., Abbatt, J. P. D., et al. (2012). Nucleation and condensational growth to CCN sizes during a sustained pristine biogenic SOA event in a forested mountain valley. *Atmospheric Chemistry and Physics*, *12*(7), 3147–3163. https://doi.org/10.5194/acp-12-3147-2012

Pöschl, U., Martin, S. T., Sinha, B., Chen, Q., Gunthe, S. S., Huffman, J. A., et al. (2010). Rainforest aerosols as biogenic nuclei of clouds and precipitation in the Amazon. *Science*, *329*(5998), 1513–1516. https://doi.org/10.1126/science.1191056

Ramasamy, S., Ida, A., Jones, C., Kato, S., Tsurumaru, H., Kishimoto, I., et al. (2016). Total OH reactivity measurement in a BVOC dominated temperate forest during a summer campaign, 2014. *Atmospheric Environment*, *131*, 41–54. https://doi.org/10.1016/j.atmosenv.2016.01.039

Riccobono, F., Schobesberger, S., Scott, C. E., Dommen, J., Ortega, I. K., Rondo, L., et al. (2014). Oxidation products of biogenic emissions contribute to nucleation of atmospheric particles. *Science*, *344*(6185), 717–721. https://doi.org/10.1126/science.1243527

Roberts, G. C., Andreae, M. O., Zhou, J., & Artaxo, P. (2001). Cloud condensation nuclei in the Amazon Basin: "Marine" conditions over a continent? *Geophysical Research Letters*, *28*(14), 2807–2810. https://doi.org/10.1029/2000GL012585

Roberts, G. C., Artaxo, P., Zhou, J., Swietlicki, E., & Andreae, M. O. (2002). Sensitivity of CCN spectra on chemical and physical properties of aerosol: A case study from the Amazon Basin. *Journal of Geophysical Research*, *107*(D20), 8070. https://doi.org/10.1029/2001JD000583

Rose, D., Gunthe, S. S., Mikhailov, E., Frank, G. P., Dusek, U., Andreae, M. O., & Pöschl, U. (2008). Calibration and measurement uncertainties of a continuous-flow cloud condensation nuclei counter (DMT-CCNC): CCN activation of ammonium sulfate and sodium chloride aerosol particles in theory and experiment. *Atmospheric Chemistry and Physics*, *8*(5), 1153–1179. https://doi.org/10.5194/acp-8-1153-2008

Rose, D., Nowak, A., Achtert, P., Wiedensohler, A., Hu, M., Shao, M., et al. (2010). Cloud condensation nuclei in polluted air and biomass burning smoke near the mega-city Guangzhou, China—Part 1: Size-resolved measurements and implications for the modeling of aerosol particle hygroscopicity and CCN activity. *Atmospheric Chemistry and Physics*, *10*(7), 3365–3383. https://doi.org/10.5194/acp-10-3365-2010

Scott, C. E., Rap, A., Spracklen, D. V., Forster, P. M., Carslaw, K. S., Mann, G. W., et al. (2014). The direct and indirect radiative effects of biogenic secondary organic aerosol. *Atmospheric Chemistry and Physics*, *14*(1), 447–470. https://doi.org/10.5194/acp-14-447-2014

Shantz, N. C., Chang, R. Y. W., Slowik, J. G., Vlasenko, A., Abbatt, J. P. D., & Leaitch, W. R. (2010). Slower CCN growth kinetics of anthropogenic aerosol compared to biogenic aerosol observed at a rural site. *Atmospheric Chemistry and Physics*, *10*(1), 299–312. https://doi.org/10.5194/acp-10-299-2010

Sihto, S. L., Mikkilä, J., Vanhanen, J., Ehn, M., Liao, L., Lehtipalo, K., et al. (2011). Seasonal variation of CCN concentrations and aerosol activation properties in boreal forest. *Atmospheric Chemistry and Physics*, *11*(24), 13,269–13,285. https://doi.org/10.5194/acp-11-13269-2011

Stolzenburg, M. R. (1988). An ultrafine aerosol size distribution measuring system, PhD thesis, University of Minnesota, USA.

Tröstl, J., Chuang, W. K., Gordon, H., Heinritzi, M., Yan, C., Molteni, U., et al. (2016). The role of low-volatility organic compounds in initial particle growth in the atmosphere. *Nature*, *533*(7604), 527–531. https://doi.org/10.1038/nature18271

Tunved, P., Ström, J., Kulmala, M., Kerminen, V. M., Dal Maso, M., Svenningson, B., et al. (2008). The natural aerosol over Northern Europe and its relation to anthropogenic emissions—Implications of important climate feedbacks. *Tellus Series B: Chemical and Physical Meteorology*, *60*(4), 473–484. https://doi.org/10.1111/j.1600-0889.2008.00363.x

Vaishya, A., Ovadnevaite, J., Bialek, J., Jennings, S. G., Ceburnis, D., & O'Dowd, C. D. (2013). Bistable effect of organic enrichment on sea spray radiative properties. *Geophysical Research Letters*, *40*, 6395–6398. https://doi.org/10.1002/2013GL058452

Wang, J., Lee, Y. N., Daum, P. H., Jayne, J., & Alexander, M. L. (2008). Effects of aerosol organics on cloud condensation nucleus (CCN) concentration and first indirect aerosol effect. *Atmospheric Chemistry and Physics*, *8*(21), 6325–6339. https://doi.org/10.5194/acp-8-6325-2008

Wexler, A. S., & Clegg, S. L. (2002). Atmospheric aerosol models for systems including the ions H^+, NH_4^+, Na^+, SO_4^{2-}, NO_3^-, Cl^-, Br^-, and H_2O. *Journal of Geophysical Research*, *107*(D14), 4207. https://doi.org/10.1029/2001JD000451

Wimmer, D., Buenrostro Mazon, S., Manninen, H. E., Kangasluoma, J., Franchin, A., Nieminen, T., et al. (2017). Direct observation of molecular clusters and nucleation mode particles in the Amazon. *Atmospheric Chemistry and Physics Discussions*, *17*, 1–37. https://doi.org/10.5194/acp-2017-782

Wu, Z. J., Poulain, L., Henning, S., Dieckmann, K., Birmili, W., Merkel, M., et al. (2013). Relating particle hygroscopicity and CCN activity to chemical composition during the HCCT-2010 field campaign. *Atmospheric Chemistry and Physics*, *13*(16), 7983–7996. https://doi.org/10.5194/acp-13-7983-2013

Yu, H., Ortega, J., Smith, J. N., Guenther, A. B., Kanawade, V. P., You, Y., et al. (2014). New particle formation and growth in an isoprene-dominated Ozark forest: From sub-5 nm to CCN-active sizes. *Aerosol Science and Technology*, *48*(12), 1285–1298. https://doi.org/10.1080/02786826.2014.984801

Zhao, J., Ortega, J., Chen, M., McMurry, P. H., & Smith, J. N. (2013). Dependence of particle nucleation and growth on high-molecular-weight gas-phase products during ozonolysis of α-pinene. *Atmospheric Chemistry and Physics*, *13*(15), 7631–7644. https://doi.org/10.5194/acp-13-7631-2013

Zhou, L., Gierens, R., Sogachev, A., Mogensen, D., Ortega, J., Smith, J. N., et al. (2015). Contribution from biogenic organic compounds to particle growth during the 2010 BEACHON-ROCS campaign in a Colorado temperate needleleaf forest. *Atmospheric Chemistry and Physics*, *15*(15), 8643–8656. https://doi.org/10.5194/acp-15-8643-2015

Zhu, C., Kawamura, K., Fukuda, Y., Mochida, M., & Iwamoto, Y. (2016). Fungal spores overwhelm biogenic organic aerosols in a midlatitudinal forest. *Atmospheric Chemistry and Physics*, *16*(11), 7497–7506. https://doi.org/10.5194/acp-16-7497-2016